OAK RIDGE NATIONAL LABORATORY LIBRARIES
3 4456 0550028 6

CENTRAL RESEARCH LIBRARY
ORNL-TM-4482

Cy 50

FAST REACTOR ANALYTICAL SHIELDING PROGRESS REPORT FOR SEPTEMBER AND OCTOBER 1973

189a No. 10318, Activity No. 04 40 01 03 1

F. R. Mynatt

[redacted]

OAK RIDGE NATIONAL LABORATORY
CENTRAL RESEARCH LIBRARY
DOCUMENT COLLECTION
LIBRARY LOAN COPY
DO NOT TRANSFER TO ANOTHER PERSON
If you wish someone else to see this document, send in name with document and the library will arrange a loan.
UCN-7969
(3 3-67)

OAK RIDGE NATIONAL LABORATORY
OPERATED BY UNION CARBIDE CORPORATION • FOR THE U.S. ATOMIC ENERGY COMMISSION

Printed in the United States of America. Available from
the U.S. Atomic Energy Commission, Technical Information Center
P.O. Box 62, Oak Ridge, Tennessee 37830
Price: Printed Copy $5.45 ; Microfiche $1.45

This report was prepared as an account of work sponsored by the United States Government. Neither the United States nor the United States Atomic Energy Commission, nor any of their employees, nor any of their contractors, subcontractors, or their employees, makes any warranty, express or implied, or assumes any legal liability or responsibility for the accuracy, completeness or usefulness of any information, apparatus, product or process disclosed, or represents that its use would not infringe privately owned rights.

ORNL-TM-4482
UC-79d - Liquid Metal Fast
Breeder Reactors Physics

Contract No. W-7405-eng-26

Neutron Physics Division

FAST REACTOR ANALYTICAL SHIELDING PROGRESS REPORT FOR SEPTEMBER AND OCTOBER 1973

189a No. 10318, Activity No. 04 40 01 03 1

Work directed by: F. R. Mynatt

Report written by:

Lorraine S. Abbott

Work performed by:

R. L. Childs*
W. W. Engle, Jr.
Margaret B. Emmett*
F. B. K. Kam**
J. Lewin
R. E. Maerker
W. A. Rhoades
S. Uchida***
L. R. Williams

*Computer Science Division of UCC Nuclear Division.
**Reactor Operations Division.
***On assignment from Hitachi Research Laboratory, Hitachi, Limited, Hitachishi, Ibaraki-ken, Japan.

MAY 1974

NOTICE This document contains information of a preliminary nature and was prepared primarily for internal use at the Oak Ridge National Laboratory. It is subject to revision or correction and therefore does not represent a final report.

OAK RIDGE NATIONAL LABORATORY
Oak Ridge, Tennessee 37830
operated by
UNION CARBIDE CORPORATION
for the
U.S. ATOMIC ENERGY COMMISSION

OAK RIDGE NATIONAL LABORATORY LIBRARIES

3 4456 0550028 6

Progress Report

September and October 1973

FAST REACTOR ANALYTICAL SHIELDING

Activity No. 04 40 01 03 1

189a No. 10318

Approved by:

C. E. Clifford
Associate Director
Reactor and Weapons Radiation Shielding
Neutron Physics Division

TABLE OF CONTENTS

Page No.

ABSTRACT ---------- vii

1. CURRENT FFTF STUDIES ---------- 1

1.1. Coupled DOT-MORSE Calculations of Radiation Streaming Through Penetrations in the Reactor Cavity Shield ------ 1

1.2. Calculation of ^{24}Na Gamma-Ray Dose Rates in Heat Exchanger Vault ---------- 10

1.3. Calculations of the Azimuthal Peaking in the Reactor Cavity Neutron Fluxes Produced by Stored Fuel ---------- 13

2. CURRENT CRBR PLANT STUDIES ---------- 15

2.1. DOT Calculations of Stored-Fuel Effects on Ex-Vessel RSP Detectors ---------- 15

3. CODE DEVELOPMENT ---------- 37

3.1. Development of DOT-IV ---------- 37

4. ANALYSIS OF THE TSF-FTR FIRST-FISSION STORED-FUEL EXPERIMENT ---------- 39

5. ANALYSIS OF TSF INCONEL EXPERIMENT ---------- 46

6. CALCULATIONS OF GAMMA-RAY HEATING IN IRON: ANALYSIS OF TSF MEASUREMENTS WITH THERMOLUMINESCENT DOSIMETERS (TLD's) ---------- 55

7. CALCULATIONS SUPPORTING THE DESIGN OF THE TSR-II LARGE-BEAM SHIELD ---------- 64

FAST REACTOR ANALYTICAL SHIELDING PROGRAM - FY 1974

	JULY	AUG	SEPT	OCT	NOV	DEC	JAN	FEB	MAR	APR	MAY	JUNE
Design and Analysis of Experiments												
FTR Iron/Poly Secondary Gamma Experiment	■	■					■	■				
FTR Inconel Experiment	■	■				■	■					
FTR Preliminary Stored-Fuel Experiment			■	■	■	■		■	■			
Demo Preliminary Stored-Fuel Experiment						■	■	■				
FTR Stored-Fuel Experiment			■	■							■	■
Demo Stored-Fuel Experiment											■	■
TLD Check Experiment	■	■	■	■								
keV Total Cross-Section Experiment					■	■	■	■	■	■	■	■
Demo Radial Shield Experiment	■	■			■	■						
Demo Lower Axial Experiment									■	■	■	■
Support Structure Streaming Experiment												■
FTR Design Support												
RCS Penetrations	■	■	■	■		■	■			■	■	■
HCS Neutron Shielding		■	■	■	■		■	■	■			
BAPS Neutrons and Gammas	■	■	■					■	■			
Center Island Shadow Shield			■	■	■							
HTS-SDO 200 Analysis		■	■	■								
Stored-Fuel 3D Coupling				■	■	■	■	■	■	■	■	■
Demo Design Support												
Lower Axial Streaming	■	■										
R-θ RSP Analysis I		■	■	■								
R-θ RSP Analysis II + TDA Analysis					■	■	■	■				
Reactor Cavity & Support System												■
R-Z Analysis of Revised Design											■	■
R-θ RSP Analysis III												■
Code Development												
DOT IV		■	■	■	■	■	■	■	■	■	■	■
COMGOM Improvement					■	■	■	■	■	■	■	■
2-D Sensitivity Code										■	■	■
FACT Improvement						■	■	■	■			
MINX-AMPX Modifications				■	■	■	■	■	■	■	■	■

ABSTRACT

Analytical shielding work performed for the fast reactor program during the months of September and October consisted of calculations for both the FFTF and the CRBR plants, continued computer code development, the partial analysis of three different TSF experiments, and calculations supporting the design of a new TSR-II beam shield. In the FFTF studies, the combined effect of multiple penetrations through the reactor cavity shield was determined, additional predictions of the ^{24}Na gamma-ray dose rates in the heat exchanger vault were made, and a preliminary three-dimensional calculation of the reactor cavity fluxes produced by the FTR stored fuel was carried out. In the CRBR studies, predictions were made of the effect of stored-fuel neutrons on the response of the ex-vessel RSP detectors. The code development work centered on selecting features to be included in the DOT-IV code. The analyses for the TSF experiments consisted of calculations of the fission detector responses observed in the TSF-FTR first-fission stored-fuel experiment; calculations of the neutron fluxes measured in the TSF inconel experiment; and calculations of the energy deposition by ^{60}Co gamma rays in iron (as measured with thermoluminescent detectors). Several calculations were also performed to predict the heating deposition and leakage dose rates associated with a proposed large-beam TSR-II shield.

1. CURRENT FFTF STUDIES

The FFTF analytical shielding studies during September and October, 1973, consisted of calculations of the combined effect of the eight penetrations in the reactor cavity shield on the maintenance deck dose rate, calculations of the SDO-200 ^{24}Na gamma-ray dose rates in the heat exchanger vault for a revised design of the 16-in.-diam duct isolation valve, and preliminary runs to investigate the adaptability of the MORSE Monte Carlo code by the calculations of three-dimensional stored-fuel neutron fluxes in the reactor cavity.

1.1. Coupled DOT-MORSE Calculations of Radiation Streaming Through Penetrations in the Reactor Cavity Shield

Work done by: Margaret B. Emmett and W. W. Engle, Jr.

Calculations performed as part of the continuing analysis of the radiation-attenuating characteristics of the FFTF reactor cavity shield and head compartment have shown the combined effect of the various pipes and ducts through the shield on the integrated neutron and gamma-ray dose rates at the maintenance deck level. The relative locations of the reactor cavity shield and the maintenance deck are shown in Fig. 1.1. Basically, the shield is a solid concrete rim that surrounds the top of the reactor vessel (from a height of about 530 cm to 630 cm). However, at eight different locations around the vessel the shield is penetrated by pipes and ducts. These penetrations, pictured in Fig. 1.2, consist of three 16-in.-diam sodium inlet lines fitting in grooves on the outer surface of the shield, a 6-in.-diam overflow line that penetrates through the full shield, a 3-in.-diam line that penetrates through the full shield and also turns within the shield, and three SISI transporter slots that slant downward through the shield from its outer surface to its inner surface. In all cases the penetrations introduce lower density regions in the radial cavity shield which might cause localized peaking of the dose rate and thereby an increased integrated dose rate at the maintenance deck level.

In the last progress report[1] the effect of each individual penetration was compared with the effect of the solid shield. It was found that the

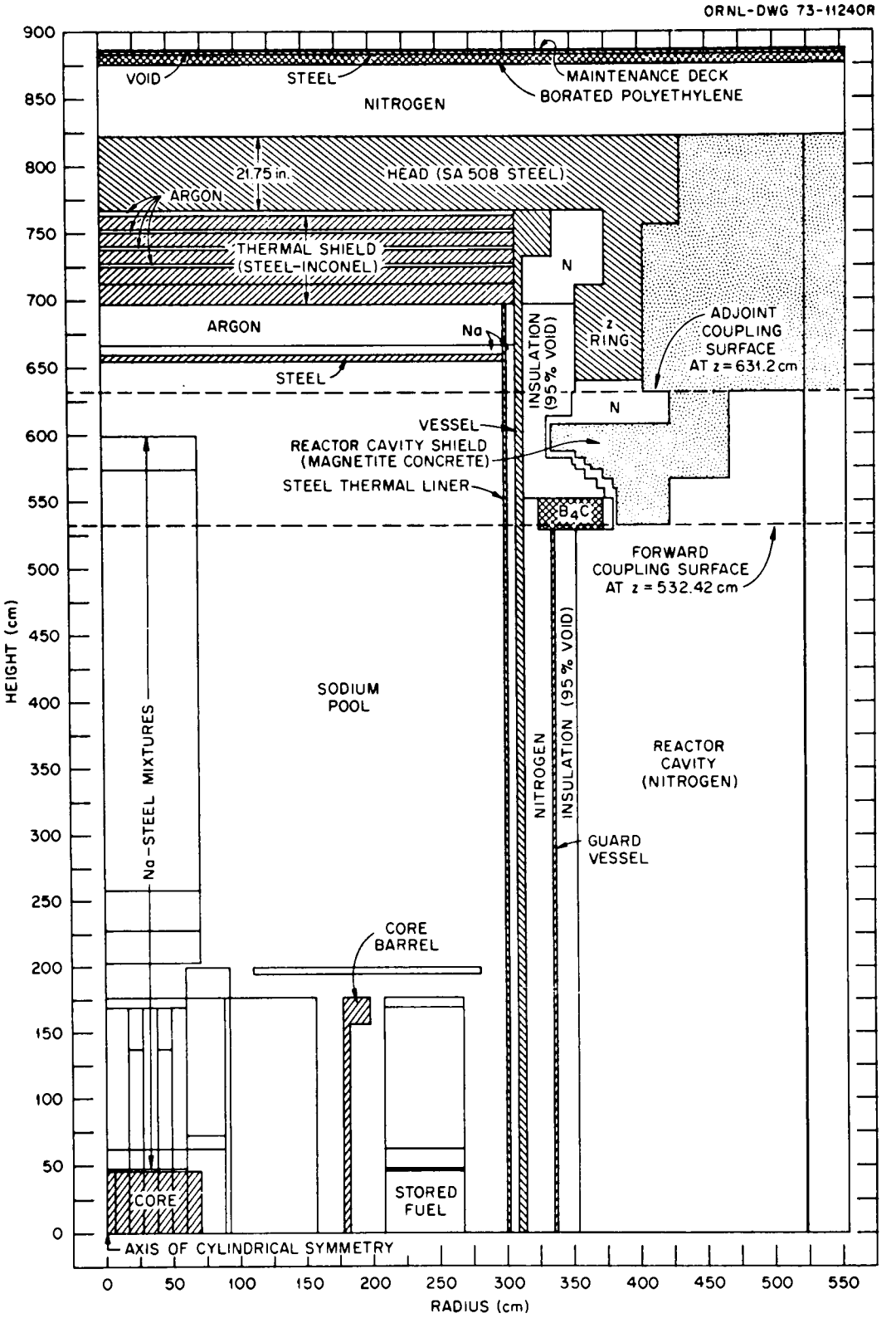

Fig. 1.1. Geometry for FTR Calculations Including Reactor Cavity Shield. Note: See Figs. 1.3 through 1.5 for variations in reactor cavity shield configuration.

ORNL-DWG 73-11451

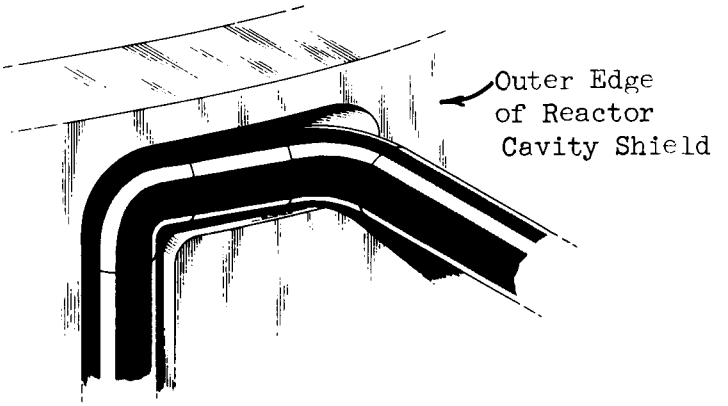

16-INCH INLET LINE

ORNL-DWG 73-11452

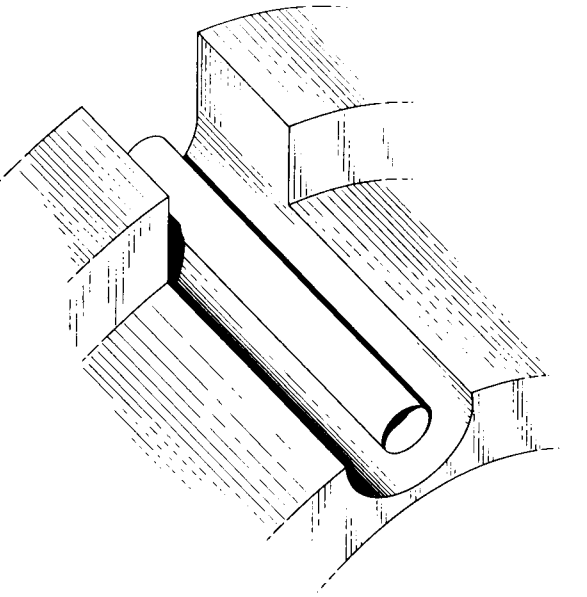

6-INCH OVERFLOW LINE

ORNL-DWG 73-11454

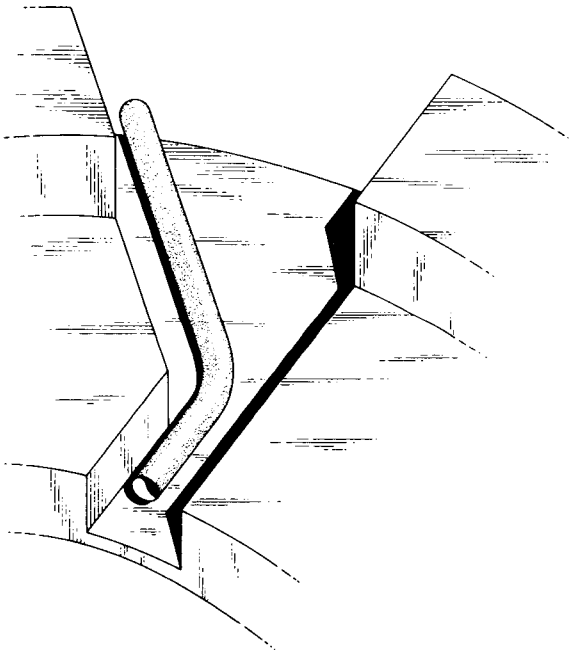

3-INCH MAKEUP LINE

ORNL-DWG 73-11453

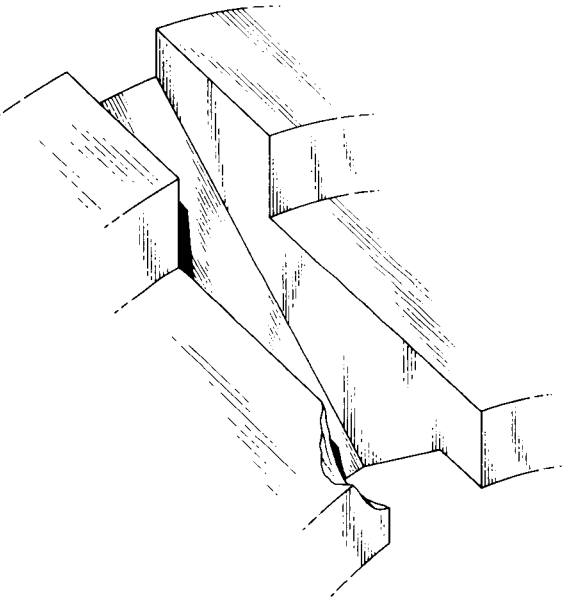

SISI TRANSPORTER SLOT

Fig. 1.2. Sketches of Various Penetrations Through Reactor Cavity Shield.

6-in. overflow line had the largest effect on the integrated gamma-ray dose, increasing it by about 14%, and the SISI transporter duct had the largest effect on the neutron dose, increasing it by about 21%. Neither of these increases is considered significant, however.

The combined effect of the eight penetrations has been calculated in the same manner as the effect of the individual penetrations. That is, the boundary angular flux at z = 532.42 cm from a forward DOT run was used by the DOMINO code to generate tables of probabilities for selecting the group, position, and direction for source neutrons for MORSE runs covering the region of the reactor cavity shield. Above the reactor cavity shield, results were used from four different adjoint DOT runs, the angular flux tapes from each having been processed by DOMINO. The sources for the adjoint calculations were the neutron flux-to-dose conversion factor and the gamma-ray flux-to-dose conversion factor, each being placed at the top of the maintenance deck and distributed radially from 260 to 450 cm in one pair of cases and from 325 to 400 cm in the other pair.

Two MORSE calculations were performed: one for the shield with the eight penetrations and one for the solid shield. It was necessary to repeat the solid-shield case here because changes have been made in the reactor cavity shield design since the calculations for the individual penetrations were performed. Also, it was erroneously stated in the last report[1] that the MORSE geometry included the steel support straps between the shield and the reactor vessel. The differences in the two solid-shield representations are shown in Fig. 1.3. The additional material introduced by including the steel support straps and reactor vessel flange and not cutting out the lower outer section of the concrete shield decreased all the integrated doses on the maintenance deck by more than a factor of four.

Changes in the reactor cavity shield configuration caused by the introduction of the 16-in. sodium inlet pipe and the 6-in. overflow line are shown in Fig. 1.4; the changes caused by the 3-in. makeup line and SISI transporter slot are shown in Fig. 1.5. A horizontal cut through the MORSE geometry at z = 601 cm shows the location of all eight penetrations (see Fig. 1.6).

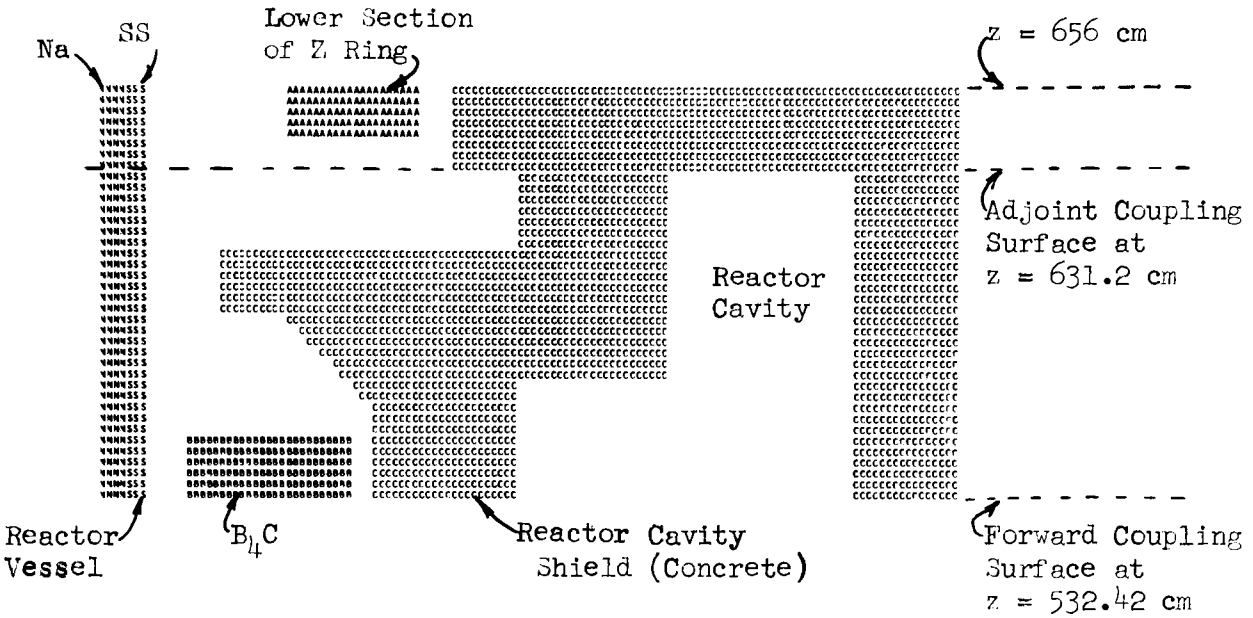

(a) Geometry for Single-Penetration Calculations (described in July-August, 1973, report, ORNL-TM-4402).

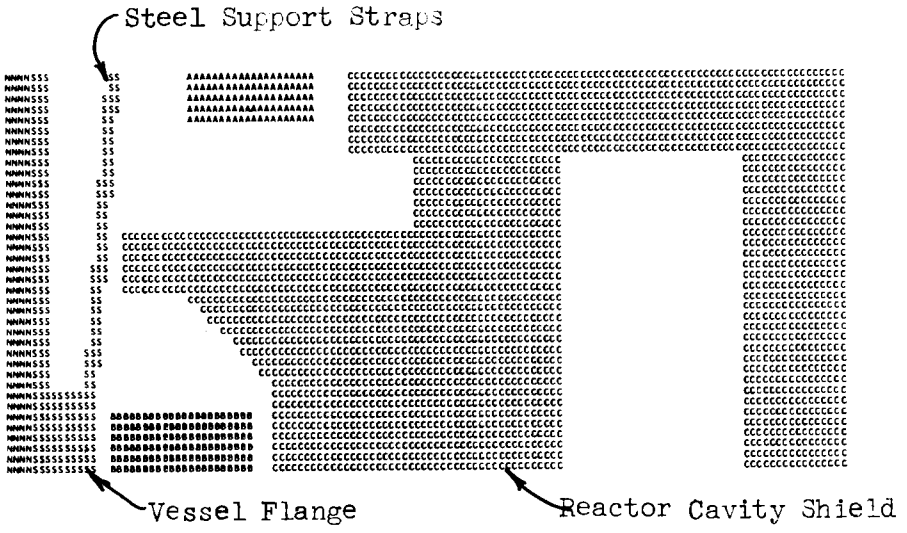

(b) Geometry for Calculations of all Eight Penetrations in Combination.

Fig. 1.3. Representations of Solid Reactor Cavity Shield in MORSE Calculations. Code: C = concrete; N = sodium; S = type 304 stainless steel; A = SA 508 steel; and B = B_4C.

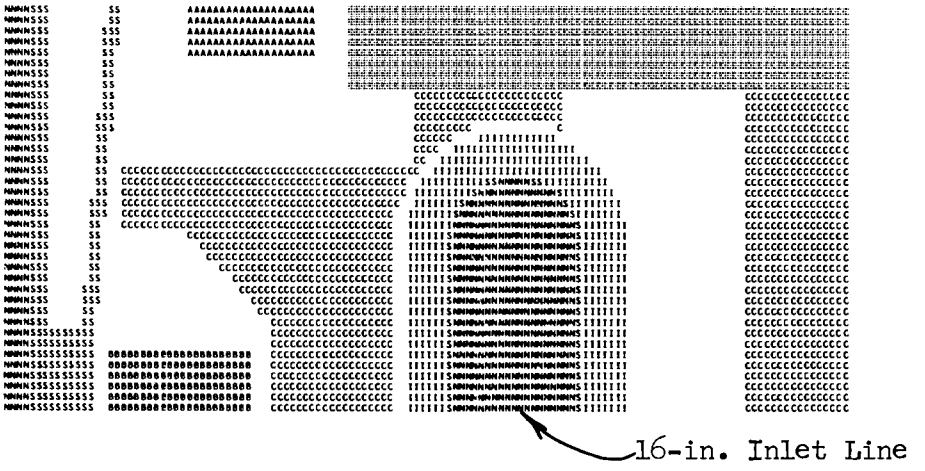

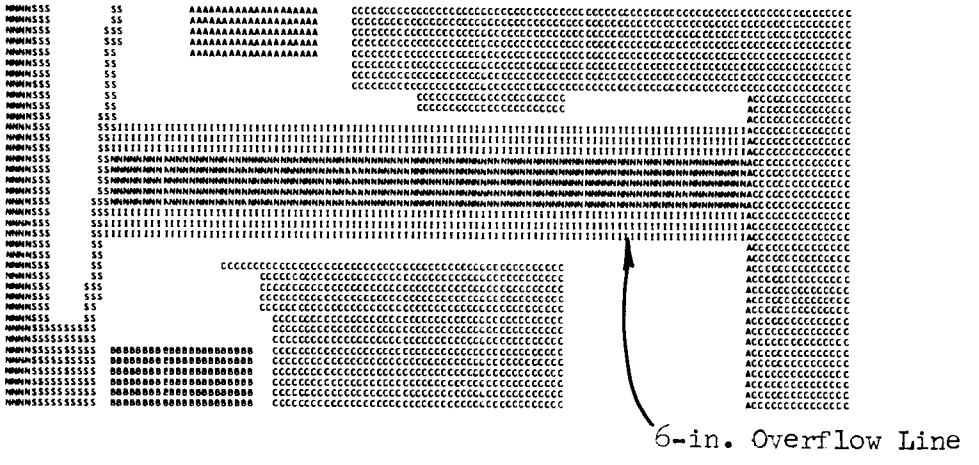

Fig. 1.4. Variations in Reactor Cavity Shield Configurations Caused by Introduction of 16-in. Inlet Line (Above) and 6-in. Overflow Line (Below). Code: C = concrete; N = sodium; S = type 304 stainless steel; A = SA 508 steel; B = B_4C; and I = insulation.

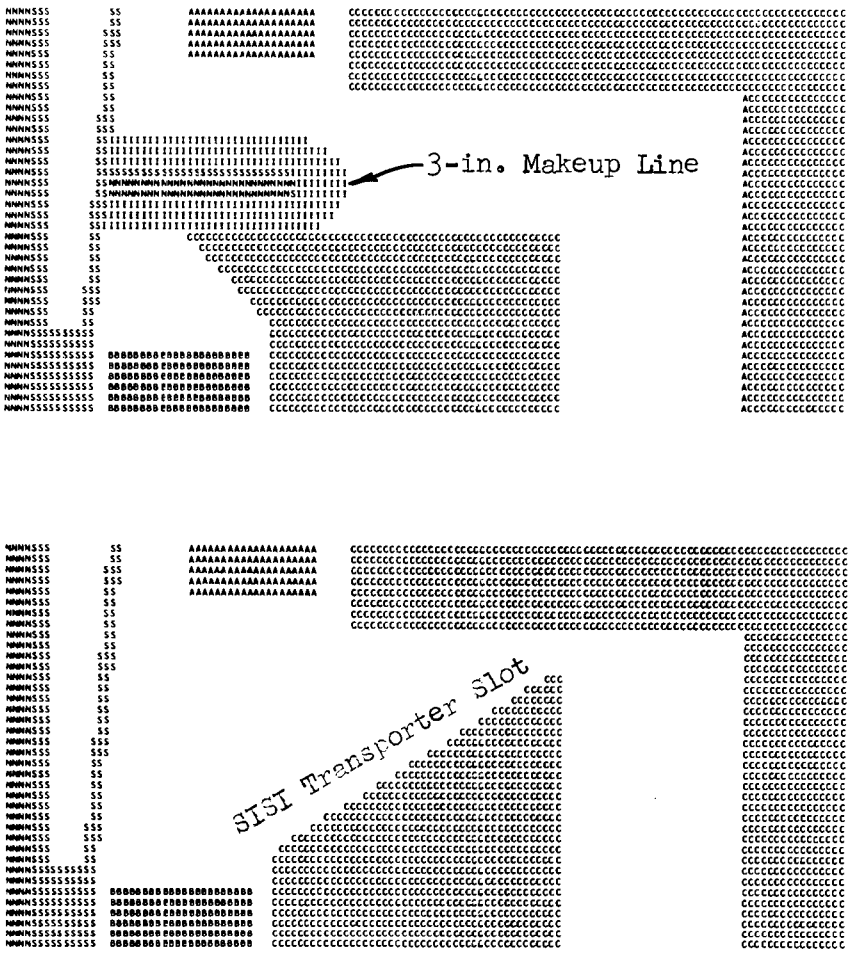

Fig. 1.5. Variations in Reactor Cavity Shield Configurations Caused by Introduction of 3-in. Makeup Line (Above) and SISI Transporter Slot (Below). Code: C = concrete; N = sodium; S = type 304 stainless steel; A = SA 508 steel; B = B_4C; and I = insulation.

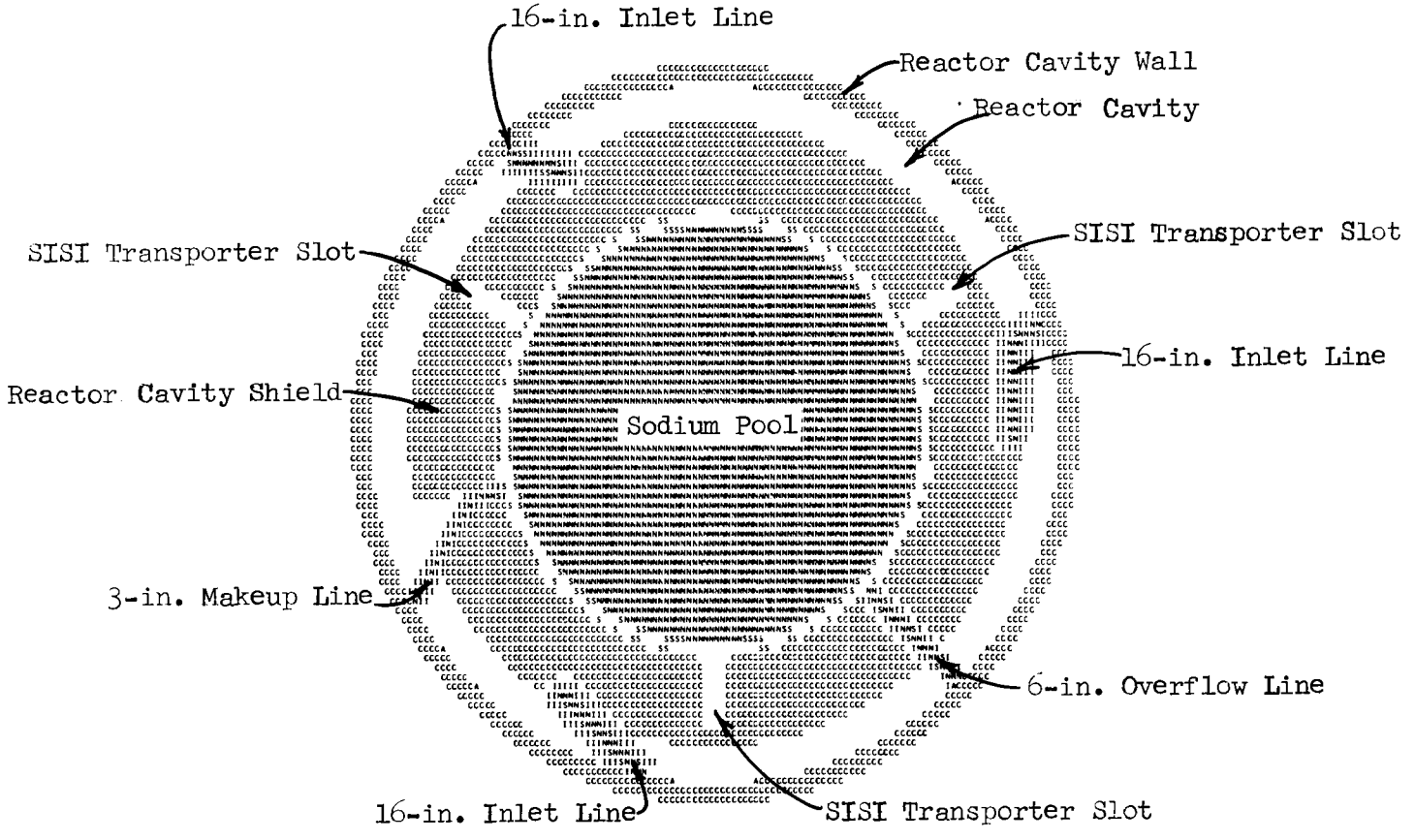

Fig. 1.6. Horizontal Cut Through FFTF Assembly at z = 601 cm. MORSE geometry including eight penetrations in reactor cavity shield. Code: C = concrete; N = sodium; S = type 304 stainless steel; I = insulation; A = SA 508 steel. Radius = 555 cm.

Table 1.1 gives the integrated dose rates on the maintenance deck for both the solid reactor cavity shield and for the shield containing all eight penetrations. The results from an all-DOT run are also included for the solid shield. When compared to the DOT solid-shield results, the integrated gamma-ray dose rates are increased by 60% by the eight penetrations; however, when compared with the coupled DOT-MORSE solid-shield results the increase is only 30%. The integrated neutron dose rates are increased 75% and 30% by the penetrations when compared with the all-DOT and DOT-MORSE solid-shield results respectively. The disagreement between the solid DOT and MORSE calculations is excessive and not well understood. Calculations of this type obviously require the development of an "adjoint difference" or "equivalent source" DOT-MORSE coupling method which will provide the ability to calculate the dose change caused by the penetrations rather than inferring the dose change by subtracting the unperturbed from the perturbed case. From these calculations the increase in the average dose on the maintenance floor is 1.5 due to these penetrations. The local peaking factor on the maintenance floor has been previously calculated to be 1.6 (ref. 1). The conservative estimate for the local dose peak on the maintenance floor is a factor of 2.4 higher than the average value for the unpenetrated reactor cavity shield.

Table 1.1. Integrated Dose Rate on FFTF Maintenance Deck with and Without Reactor Cavity Shield Penetrations

Configuration	Integrated Dose Rate (cm^2-mrem/hr) Gamma Rays	Neutrons
Adjoint Source at R = 260-450 cm		
Solid shield (DOT)	1.37+5	1.53+5
Solid shield (DOT-MORSE)	1.70+5(0.06)*	2.07+5(0.09)
Shield with eight penetrations (DOT-MORSE)	2.20+5(0.10)	2.69+5(0.16)
Adjoint Source at R = 325-400 cm		
Solid shield (DOT)	7.00+4	9.40+4
Solid shield (DOT-MORSE)	8.72+4(0.06)	1.28+5(0.10)
Shield with eight penetrations (DOT-MORSE)	1.12+5(0.10)	1.64+5(0.16)

*Read: 1.70×10^5 cm^2-mrem/hr with 6% fractional standard deviations.

1.2. Calculations of ^{24}Na Gamma-Ray Dose Rates in Heat Exchanger Vault

Work done by: Margaret B. Emmett and W. W. Engle, Jr.

During this reporting period several additional Monte Carlo (MORSE) calculations were performed to predict what the ^{24}Na gamma-ray dose rates in the heat exchanger vault would be if stainless steel shield patches of a slightly different design were used along the edges of the pipe chases on both sides of the 27-in.-thick shadow shield wall.* The criterion, referred to as the SDO-200 condition, has been that at zero time after shutdown the dose rate not exceed 200 mrem/hr at any location in the vault when the isolation valves on the adjacent HTS pipeway have been closed long enough for the sodium in the pipes beyond the valves to decay (during operation at two-thirds power). Earlier calculations[2] (by F. B. K. Kam) for the case of a shorter isolation valve for the 16-in.-diam pipe had shown that even with patches the dose rates in the vault near the edge of the 16-in.-diam inlet pipe would be 1170 mrem/hr, which is almost a factor of six too high. Since this region of the vault presents the most serious problem, these new calculations were also performed for the case of the 16-in. pipe entrance into the vault.

The three-dimensional geometry assumed for the calculations is shown in Fig. 1.7. The activated source, taken to be 14 miC/cm^3, was restricted to the reactor side of the isolation valve. The patches within the pipeway consisted of two 40-in.-high stainless steel slabs, one 6 by 9 in. and the other 6 by 12 in. The patches within the vault were large annular rings, the one adjacent to the wall having an inside diameter equivalent to the diameter of the pipe chase. The diameter of the other cylinder was 24 in.

Three detector positions were considered as shown in the lower left-hand corner of Fig. 1.7. Detectors 1 and 3 were in the horizontal midplane of the pipe, and Detector 2 was above the pipe on the inside surface of the largest annular steel ring (see inset in figure). (In the coordinate system used, x,y,z = 0 at the center of the reactor core.)

*The shadow shield wall was originally designed to be constructed of magnetite concrete and to have a thickness of 33 in., but it was changed to magshot and reduced to 24 in. about mid-1973.

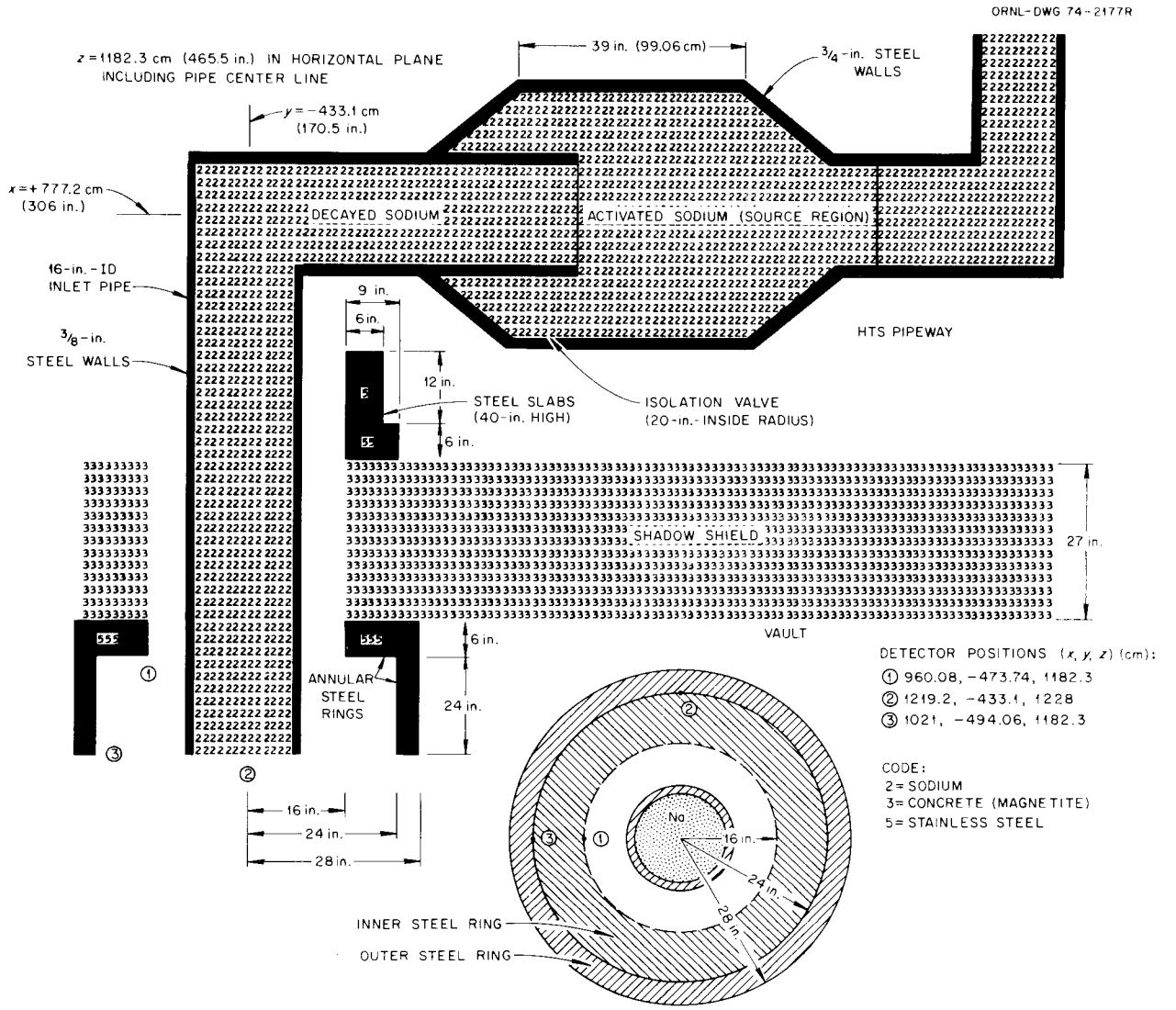

Fig. 1.7. Geometry for MORSE Calculations of ^{24}Na Gamma-Ray Dose Rates in FFTF Heat Exchanger Vault.

The dose rates for the three locations are given in Table 1.2. Only the dose rate at Detector 2 is below the design criterion, the value for Detector 1 being too high by a factor of five and the value for Detector 2 being too high by a factor of two. In view of these results, ARD re-examined the maintenance requirements for the heat exchanger vault and determined that access to the high dose-rate regions would not be necessary. Therefore, the regions near the pipe chases were designated as exclusion areas in which the dose rate could exceed 200 mrem/hr. The shadow shield design was then released to the contractors with all the stainless steel patches included except the 24-in.-ID ring.

Table 1.2. ^{24}Na Gamma-Ray Dose Rates in FFTF Heat Exchanger Vault (See Fig. 1.7 for detector locations.)

	Henderson Dose Rate (mrem/hr)	
Detector	Uncollided	Total
1	89.3 (0.04)*	1072.3 (0.36)
2	0.23 (0.01)	109.98 (0.44)
3	0.0101 (0.08)	406.44 (0.31)

*Number in parentheses indicates per cent standard deviation.

1.3. Calculations of Azimuthal Peaking in the Reactor Cavity Neutron Fluxes Produced by Stored Fuel

Work done by: Margaret B. Emmett and W. W. Engle, Jr.

During this period a few preliminary Monte Carlo MORSE runs were performed to investigate a technique for calculating the neutron fluxes in the FFTF reactor cavity produced by the stored fuel. The source used for these runs was the power in each of 22 elements in a stored-fuel module which had been determined from an earlier DOT calculation in r-θ geometry.[3] Two detector positions in the cavity were considered, both located in the FTR core horizontal midplane. One detector was opposite the stored-fuel module and the other was about halfway between two modules. All the calculations were carried out in the forward mode.

The results indicated that the MORSE code was adaptable to this type of calculation. Therefore, work has begun to describe the system in COMGOM[4] rather than in general geometry. Once this has been done, the calculation can be performed much faster and changes in the description of the stored-fuel module can be introduced with a minimum of effort. The plan is to perform a series of calculations which will yield the average value of the flux and the azimuthal flux shape at a given radius and given height in the cavity.

Section 1. References

1. F. R. Mynatt *et al.*, "Fast Reactor Analytical Shielding Progress Report for July and August, 1973," ORNL-TM-4402 (November 1973).

2. ORNL-TM-4402 *op cit.*, p. 15.

3. F. R. Mynatt *et al.*, "Fast Reactor Analytical Shielding Progress Report for May and June 1973," ORNL-TM-4401, p. 43 (February 1973).

4. E. A. Straker, W. H. Scott, Jr., and N. R. Byrn, "The MORSE Code with Combinatorial Geometry," DNA 2860T (SAI-72-511-LJ) (May 1972).

2. CURRENT CRBR PLANT STUDIES

2.1. DOT Calculations of Stored-Fuel Effects on Ex-Vessel RSP Detectors

Work done by: W. W. Engle, Jr., L. R. Williams, and F. R. Mynatt

Our most recent studies for the Clinch River Breeder Reactor Project (CRBR), has consisted of a series of DOT calculations to determine the adequacy of the ex-vessel RSP detectors (reactor surveillance procedure) monitoring the shutdown reactor in the presence of neutrons from stored fuel elements. If the monitors are to be effective, the ratio of the background from stored-fuel neutrons must not be excessive. The present criterion is that the stored-fuel background should not exceed 10% of the counts from the core.

The CRBR fuel elements are to be arranged in a hexagonally shaped core consisting of an inner region and an outer region whose elements differ slightly in composition. The two regions are shown in Fig. 2.1. In the present design the core is surrounded by a radial blanket of depleted uranium oxide, a radial reflector of stainless steel, and a radial restraint region of inconel. Around the entire assembly is a 14-in.-thick steel shield, with all the regions, including the shield, enclosed in the core barrel. The materials in the various regions are given in Tables 2.1 - 2.4, including the materials for the control rods. The control-rod positions are indicated in Fig. 2.1 by the "+'s" in the inner core.

When the first DOT calculations were performed, the plant design in the region outside the core barrel was also as shown in Fig. 2.1. It provided for the storage of as many as 36 used fuel elements in three "stored-fuel modules" placed symmetrically around the core barrel within steel shields. In between the modules, but outside the reactor vessel, are three clusters of ^{235}U fission detectors serving as neutron-flux monitors during reactor shutdown. Since these detectors are sensitive primarily to low-energy neutrons, the five detectors in each cluster are embedded in a material (graphite) that moderates the incident fast neutrons. The box is shielded on three sides with B_4C. The compositions of these

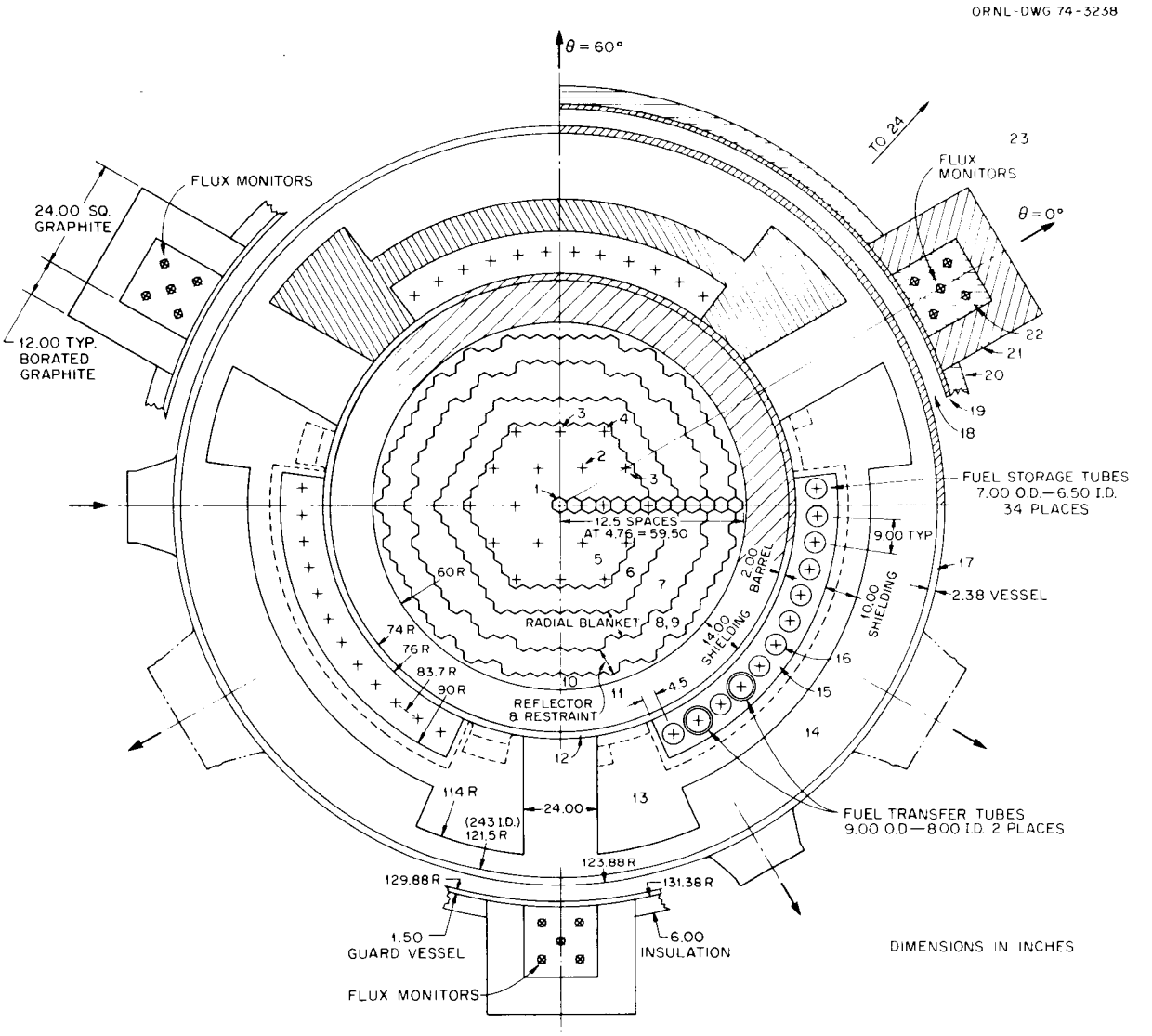

Fig. 2.1. Horizontal Cross Section of CRBR Reactor Vessel Through Midplane of Core. See Table 2.1 for identification of numbered regions. r,θ calculations were performed for θ = 0 to 60 deg to determine response of flux monitors to neutrons from shutdown core and stored-fuel elements.

Table 2.1. Identification of Radial Regions Through Horizontal Midplane of CRBR Reactor Core (See Fig. 2.1)

Region Number	Identification	Composition
1	Center control rod	See Table 2.2
2	Row 4 control rods	"
3,4	Row 7 control rods	"
5	Inner core	See Table 2.3
6	Outer core	"
7	Radial blanket	"
8	Reflector	See Table 2.4
9	Radial restraint	"
10	Sodium	Average density = 2.186×10^{-2} atoms/b·cm
11	Radial shield	See Table 2.4
12	Core barrel	"
13	Stored-fuel shield	"
14,15	Sodium	See above
16	Stored-fuel element	See Table 2.3
17	Reactor vessel	See Table 2.4
18,23	Cavity	Nitrogen, density = 5.38×10^{-5} atoms/b·cm
19	Guard vessel	See Table 2.4
20	Insulation	0.061 vol% $CaSiO_3$
21	B_4C shield	B_4C, boron density = 9.37×10^{-2} atoms/b·cm, carbin density = 2.34×10^{-2} atoms/b·cm
22	Graphite[a]	Carbon density = 1.1284×10^{-1} atoms/b·cm
24	Reactor cavity wall	Magnetite concrete (see Table 2.5)

[a]The carbon density used in the calculation was 2.25 g/cc; it should have been 1.6 g/cc, but the difference would not be expected to change the relative responses of the detectors.

various regions are given in Tables 2.1 and 2.4.

Table 2.2. Assumed Compositions of CRBR Control Rod Regions[a] (See Fig. 2.1)

Nuclide	Atomic Density (atoms/b·cm)		
	Natural Boron Control Rods (Regions 1, 3, 4)	40% Enriched Boron Control Rods (Region 2)	Control Channel[b]
^{10}B	7.177(-3)[c]	1.473(-2)	
^{11}B	2.911(-2)	2.209(-2)	
C	9.072(-3)	9.206(-3)	
Na	7.334(-3)	7.334(-3)	2.053(-2)
Cr	4.4(-3)	4.4(-3)	1.497(-3)
Fe	1.709(-2)	1.709(-2)	5.814(-3)
Ni	2.75(-3)	2.75(-3)	9.335(-4)

[a]For cases in which control rods were partially withdrawn, the control rod and control channel were mixed with appropriate volume fractions.
[b]With control rod fully withdrawn.
[c]Read: 7.177×10^{-3}.

As pointed out above, the effectiveness of the monitors depends on the degree to which they are protected from stored-fuel neutrons. In an attempt to minimize the transport of neutrons from the stored fuel to the detectors, the steel shield around each stored-fuel module was thickened on each end.

Four cases were calculated to determine the fission counter responses for the geometry shown in Fig. 2.1. The first two cases were for the reactor at full power (900 MW_{th}) with and without neutrons from the stored fuel considered, and the next two cases were for the reactor shut down

Table 2.3. Assumed Compositions of CRBR Fueled Radial Regions (See Fig. 2.1)

Nuclide	Atomic Density (atoms/b·cm) Inner Core (Region 5)	Outer Core (Regions 6, 16)	Radial Blanket (Region 7)
^{239}Pu	8.229(-4)[a]	1.1927(-3)	
^{240}Pu	2.9674(-4)	4.3021(-4)	
^{241}Pu	1.7555(-4)	2.5427(-5)	
^{242}Pu	5.407(-5)	7.834(-5)	
^{235}U	1.172(-5)	1.059(-5)	2.65(-5)
^{238}U	5.8705(-3)	5.2863(-3)	1.323(-1)
O	1.433(-2)	1.438(-2)	2.625(-2)
Na	8.8865(-3)	8.916(-3)	5.451(-3)
Ni	2.2277(-3)	2.277(-3)	1.558(-3)
Cr	3.642(-3)	3.642(-3)	2.492(-3)
Fe	1.416(-3)	1.416(-3)	9.689(-3)

[a]Read: 8.229×10^{-4}.

Table 2.4. Assumed Compositions of CRBR Nonfueled Radial Regions (See Fig. 2.1)

Nuclide	Atomic Density (atom/b·cm) Reflector (Region 8)	Radial Restraint (Region 9)	Type 304 Stainless Steel (Regions 11, 12, 13, 17, 19)
Na	2.6567(-3)[a]	-	-
Cr	1.55317(-2)	1.52928(-2)	1.74(-2)
Fe	5.38472(-2)	1.24585(-2)	5.96(-2)
Ni	7.4207(-3)	5.92548(-2)[b]	7.7(-3)
Mn			1.3(-3)

[a]Read: 2.6567×10^{-3}.

[b]Weighted $1/E\ \sigma_t$.

with and without neutrons from the stored fuel considered. Source data for the shutdown cases are given in Table 2.6 and the source energy spectra are given in Table 2.7 in the standard 50-group structure used for earlier FTR calculations. The two spectra correspond to the shutdown "inherent"

Table 2.5. Assumed Composition of Magnetite Concrete Used in CRBR Cavity Wall[a]

Element	Density (g/cc)	Atomic Density (atom/b·cm)
Hydrogen	0.012[b]	7.17(-3)[b,c]
Oxygen	1.1634	4.379(-2)
Iron	1.4982	1.616(-2)
Titanium	0.3566	4.48(-3)
Vanadium	0.0098	1.2(-4)
Silicon	0.0765	1.64(-3)
Aluminum	0.0618	1.38(-3)
Magnesium	0.0107	2.7(-4)
Calcium	0.1640	2.47(-3)
Sulphur	0.0029	6.0(-5)
Carbon	0.0011	6.0(-5)
Sodium	0.0012	3.0(-5)
Other	0.0004	
Total	3.3641	7.763(-2)

[a]Except where noted, composition was given in FRP-770 (March 8, 1972). Note: Current plans are to use ordinary concrete for the cavity wall, but for this calculation the differences in the two concrete compositions would have little effect on the results.
[b]Hydrogen densities given in FRP-811 (April 12, 1972).
[c]Read: 7.17×10^{-3}.

source and the shutdown "fission" source respectively. The inherent source consists of neutrons produced by the spontaneous fission of plutonium and by oxygen (α,n) reactions. The fission source consists of neutrons produced when the inherent source neutrons induce fissions in the plutonium or uranium (that is, the multiplied source). For the purposes of these calculations, the plutonium fission spectrum was used.

The DOT calculations used the 50-group FTR cross sections, an S_6 quadrature, and P_1 scattering. They were performed in r,θ geometry, the $\theta = 0$ position being along a line connecting the core center and the central detector. The region covered was from $\theta = 0$ to 60 deg, which was the smallest symmetrical region that could be examined (see Fig. 2.1). Along the radius the geometry extended past the flux monitors through the nitrogen-filled cavity surrounding the reactor vessel and 1 ft into the concrete reactor cavity wall (concrete composition given in Table 2.5).

The initial calculations in this study were performed in two steps, the first step covering the region from the core center to the outer radius of the radial shield (to r = 74 in.). The second step covered the remaining regions, using as the source a boundary angular flux from the first step. Later the full geometry was handled in a single run.

Table 2.6. Source Data for CRBR Shutdown Cases

Stored-Fuel Inherent Source	1.8×10^5 neutrons/sec
Stored-Fuel Fission Source	1.35×10^5 neutrons/sec
Core Inherent Source	8.24×10^5 neutrons/sec
Core Fission Source	8.44×10^6 neutrons/sec
K_{eff} of Stored Fuel	0.429
K_{eff} of Core	0.911

Table 2.9. Spectra of Inherent and Fission Sources Used for CRBR Shutdown Cases

Group No.	Upper Energy Limit (MeV)	Neutrons/Group	
		Inherent Source[a]	Fission Source[b]
1	1.4918(1)[c]	2.784(-3)	1.8567(-4)
2	1.2214(1)	4.913(-3)	1.0122(-3)
3	1.0000(1)	7.323(-3)	3.7899(-3)
4	8.1873(0)	1.3521(-2)	1.0441(-2)
5	6.7032(0)	2.2719(-2)	2.2400(-2)
6	5.4881(0)	3.8223(-2)	3.9215(-2)
7	4.4933(0)	5.7777(-2)	5.8216(-2)
8	3.6788(0)	8.7764(-2)	7.5625(-2)
9	3.0119(0)	1.0021(-1)	8.8198(-2)
10	2.4660(0)	1.0676(-1)	9.4291(-2)
11	2.0190(0)	9.7356(-2)	9.3976(-2)
12	1.6530(0)	8.2668(-2)	8.8512(-2)
13	1.3533(0)	7.0785(-2)	7.9651(-2)
14	1.1080(0)	5.9885(-2)	6.9089(-2)
15	9.0718(-1)	5.1314(-2)	5.8175(-2)
16	7.4274(-1)	4.7029(-2)	4.7824(-2)
17	6.0810(-1)	3.6002(-2)	3.8558(-2)
18	4.9787(-1)	2.8846(-2)	3.0602(-2)
19	4.0762(-1)	2.3119(-2)	2.3980(-2)
20	3.3373(-1)	1.7139(-2)	1.8597(-2)
21	2.7324(-1)	1.3100(-2)	1.4302(-2)
22	2.2371(-1)	9.498(-3)	1.0923(-2)
23	1.8316(-1)	7.205(-3)	8.2960(-3)
24	1.4996(-1)	5.404(-3)	6.2722(-3)
25	1.2277(-1)	3.766(-3)	7.4788(-3)
26	8.6517(-2)	2.047(-3)	5.8508(-3)
27	5.2475(-2)	1.146(-3)	1.6638(-3)
28	4.0868(-2)	7.86(-4)	1.1514(-3)
29	3.1828(-2)	5.40(-4)	7.9564(-4)
30	2.4787(-2)	3.77(-4)	5.4913(-4)
31	1.9304(-2)	0	3.7865(-4)
32-50	1.5034(-2)	0	0

[a]Neutrons due to spontaneous fission of plutonium and to oxygen (α,n) reactions.

[b]Neutrons produced by fissions induced in Pu and U by inherent-source neutrons. Spectrum given here is ^{239}Pu spectrum; it is used as the spectrum for fission neutrons from both Pu and U.

[c]Read: 1.4918×10^{1}.

The r,θ grids used for the calculations were selected to match the edges of the various CRBR regions as closely as possible. For Regions 1 - 10, which had irregular edges because of their hexagonally shaped components, this required bracketing the edges of the regions with the radial and theta intervals. The resulting grid is shown in Fig. 2.2, in which the heavy lines represent the edges of the regions. With these lines used as a guide, the regional boundaries shown in Fig. 2.3 were chosen for the calculations. The grid shown in Figs. 2.2 and 2.3 (also defined in Table 2.8) was used for the first step in the two-step calculation. The same radial intervals were used for the full-geometry calculations, but the theta intervals were revised slightly.

Table 2. 8. r,θ Grid Descriptions for CRBR Calculation of Radial Regions 1-10 (See Figs. 2.2 and 2.3)

Radial Intervals					
Outer Radius		No. of Intervals	Interval Width		Interval Numbers
(in.)	(cm)		(in.)	(cm)	
4.76	12.0904	4	1.19	3.0226	1-4
9.52	24.1808	2	2.38	6.0452	5-6
16.66	42.3164	6	1.19	3.0226	7-12
21.42	54.4068	2	2.38	6.0452	13-14
45.22	114.8588	20	1.19	3.0226	15-34
59.50	151.130	24	0.595	1.5113	35-58
60.00	152.40	2	0.25	0.635	59-60
72.00	182.88	12	1.00	2.54	61-72
74.00	187.96	4	0.5	1.27	73-76

Theta Intervals

Theta boundaries were 0 and 60 deg in thirty 2-deg intervals.

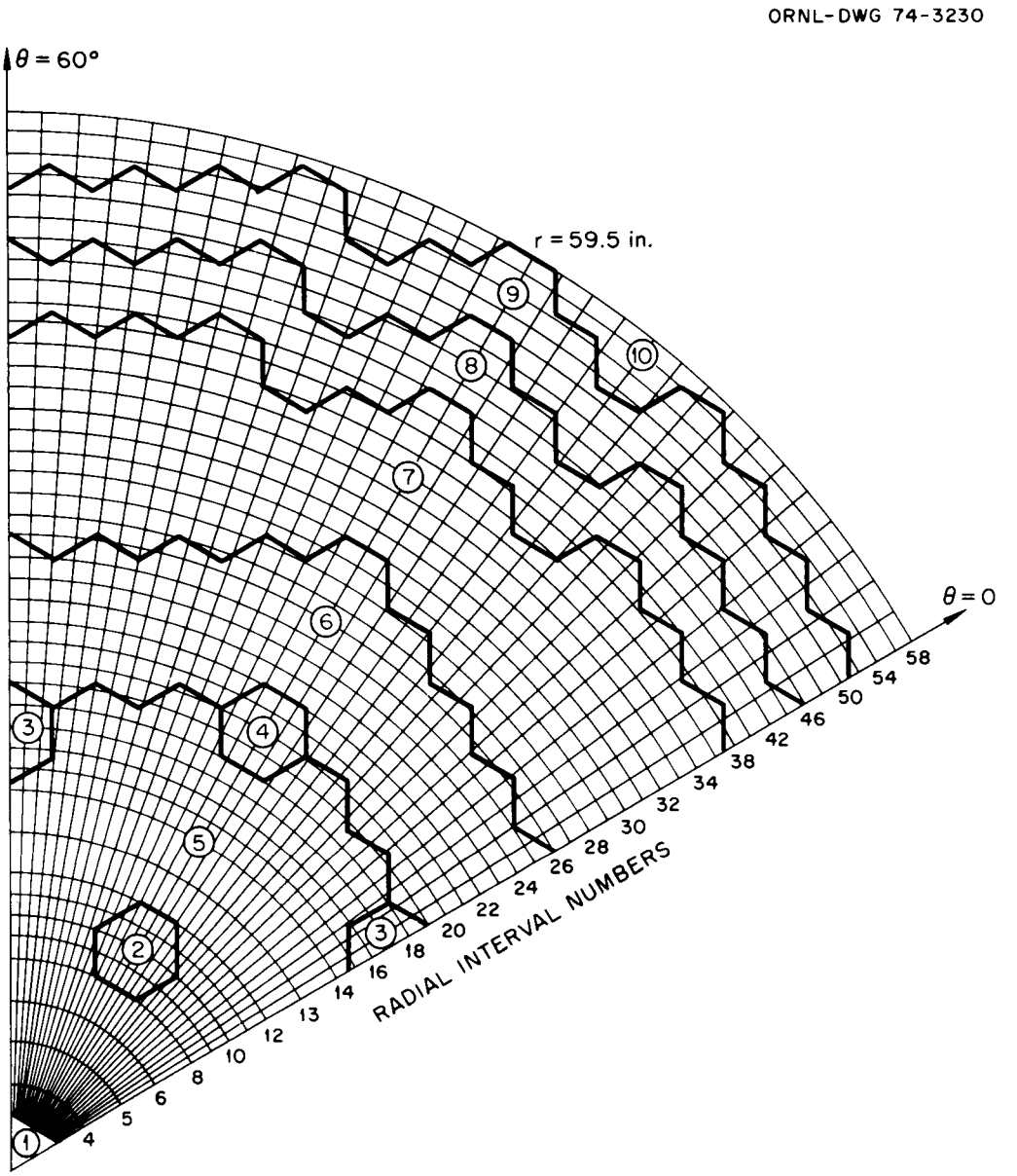

Fig. 2.2. r,θ Grid with Overlay of CRBR Radial Regions 1-10. See Table 2.8.

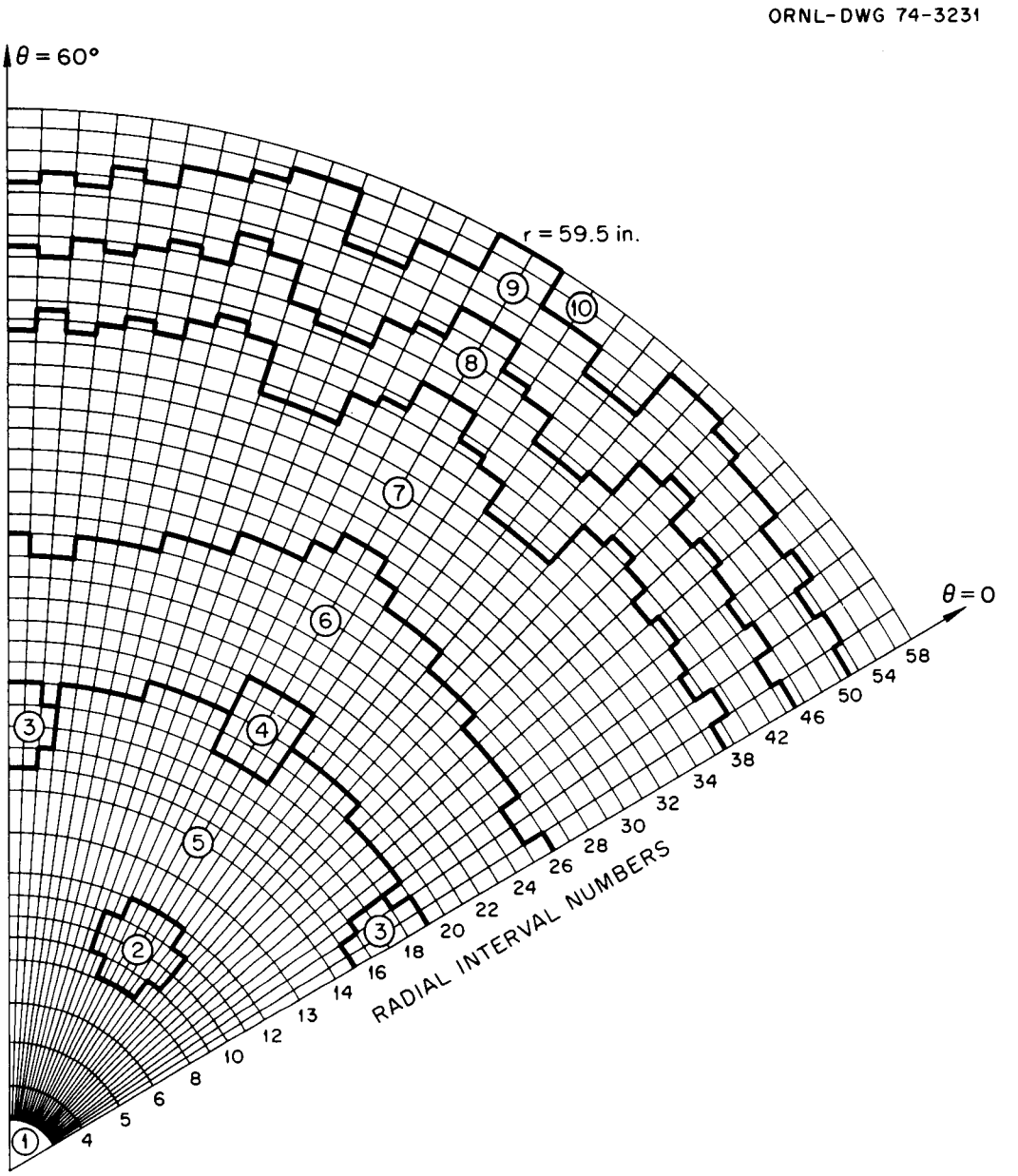

Fig. 2.3. r,θ Grid with Overlay of CRBR Radial Regions 1-10 as Mocked Up in Calculations. See Table 2.8.

The r,θ grid selected for the second step of the two-step calculations is shown in Fig. 2.4 and Table 2.9. In this case the radial intervals coincide with the region boundaries. In the case of the stored-fuel elements, the theta intervals were assumed also to coincide with the region boundaries; however, in the cases of the stored-fuel shield and detector box, the edges were represented by stepped theta intervals. In this calculation more theta intervals are required in order to accurately mock up the flux monitor box and the stored-fuel module. The radial intervals shown here were also used in the full-geometry calculation. The theta intervals for the full-geometry calculations were very similar to these, but some modification of the theta grid was required to handle all the CRBR regions simultaneously. Most of the results given below are from the full-geometry runs, Figs. 2.2 through 2.4 being presented only to help the reader visualize the problem.

As is apparent from our previous progress reports, the detailed results from DOT calculations are most conveniently presented as "isoplots" of the calculated responses over various regions of the geometry. At the time these calculations were performed we did not have a capability for generating isoplots in r,θ geometries. The results from these calculations are presented as isoplots on an x,y geometry, where the x axis represents the radius and the y axis represents the theta direction measured in revolutions (60 deg = 0.167 revolutions). An x,y representation of the regions beyond the reflector is shown in Fig. 2.5. Although in this representation the theta scale is distorted, the isoplots presented over this geometry will be accurate for given values of r and θ.

Isoplots for the two shutdown cases, that is, with and without the stored fuel, are presented in Figs. 2.6 through 2.9. Figures 2.6 and 2.7 show the total neutron flux, and Figs. 2.8 and 2.9 show the reaction rate for a ^{235}U detector. Comparisons of the corresponding curves reveal that the stored fuel has a significant effect on the responses in the vicinity of the flux monitors.

The reaction rates and count rates for the centermost detector determined from these two shutdown cases are given in Table 2.10, along with corresponding values for the at-power cases. The results show that when the reactor is shut down, the ratio of the count rates due to stored-fuel neutrons to the count rate due to core neutrons is about 17 to 1, which is unacceptable. Even when the reactor is at full power, neutrons from the stored fuel have a small but noticeable effect on the monitor.

In order to get some idea of whether the fission detectors could be sufficiently shielded from the stored-fuel neutrons, additional shutdown cases were calculated for a geometry in which the B_4C shielding around the graphite was extended inward to the core barrel as shown in Fig. 2.10 (a structurally impractical case). The results for these cases, presented in the third line of Table 2.2, show that the fission detector would count 2.5 core neutrons for every stored-fuel neutron, which is a great improvement but still not satisfactory. This hypothetical configuration is an upper limit in shielding the detectors from the stored fuel.

Finally, shutdown cases were run for a revised ARD design in which the thickness of the ends of the fuel module shield was increased and the reactor vessel was surrounded by a B_4C shield (see Fig. 2.11). The results, shown in the last line of Table 2.10, still are not satisfactory and indicate that an adequate shield design for the stored-fuel modules may not be possible. The inclusion of the stored-fuel modules in this region of the CRBR plant is therefore in question.

ORNL-DWG 74-3237

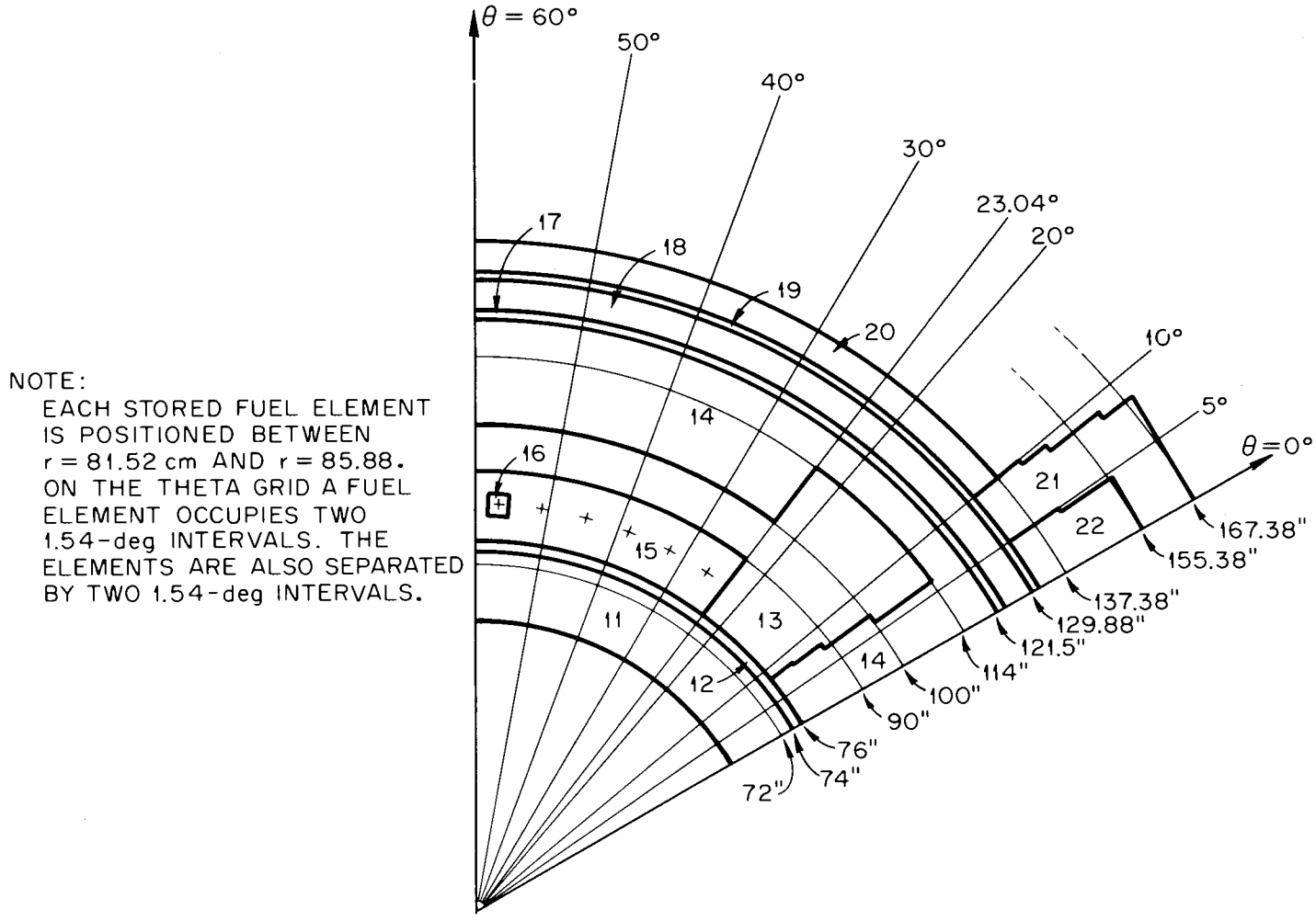

Fig. 2.4. r,θ Grid Overlay of CRBR Radial Regions 11-23. See Table 2.9. Radial intervals actually extended to 252 in., which included 1 ft of the concrete cavity wall.

Table 2.9. r,θ Grid Descriptions for CRBR Calculation of Radial Regions 11-24 (See Fig. 2.4)

Radial Intervals					
Outer Radius[a]		No. of Intervals	Interval Width		Interval Numbers
(in.)	(cm)		(in.)	(cm)	
74	187.96	2	1.0	2.54	1-2
76	193.04	4	0.5	1.27	3-6
81.52	207.0608	2	2.76	7.0104	7-8
83.70	212.5980	1	2.18	5.5372	9
85.88	218.1352	1	2.18	5.5372	10
90.0	228.60	2	2.06	5.2324	11-12
100.0	254.0	4	2.50	6.35	13-16
114.0	289.56	7	2.0	5.08	17-23
121.50	308.61	2	3.75	9.525	24-25
123.88	314.6552	2	1.19	3.0226	26-27
129.88	329.8952	1	6.0	15.24	28
131.38	333.7052	2	0.75	1.905	29-30
137.38	348.9452	6	1.00	2.54	31-36
167.38	425.1452	30	1.00	2.54	37-66
180.0	457.20	2	6.31	16.0274	67-68
192.0	487.68	1	12.0	30.48	69
240.0	609.60	2	24.0	60.96	70-71
241.0	612.14	2	0.5	1.27	72-73
243.0	617.22	2	1.0	2.54	74-75
252.0	640.08	3	3.0	7.62	76-78

Theta Intervals			
θ (deg)	No. of Intervals	Interval Width (deg)	Interval Numbers
0-10	20	0.5	1-20
10-20	5	2.0	21-25
20-23.04	2	1.52	26-27
23.04-60	24	1.54	28-51

[a]Calculation begins at r = 72 in. = 182.88 cm.

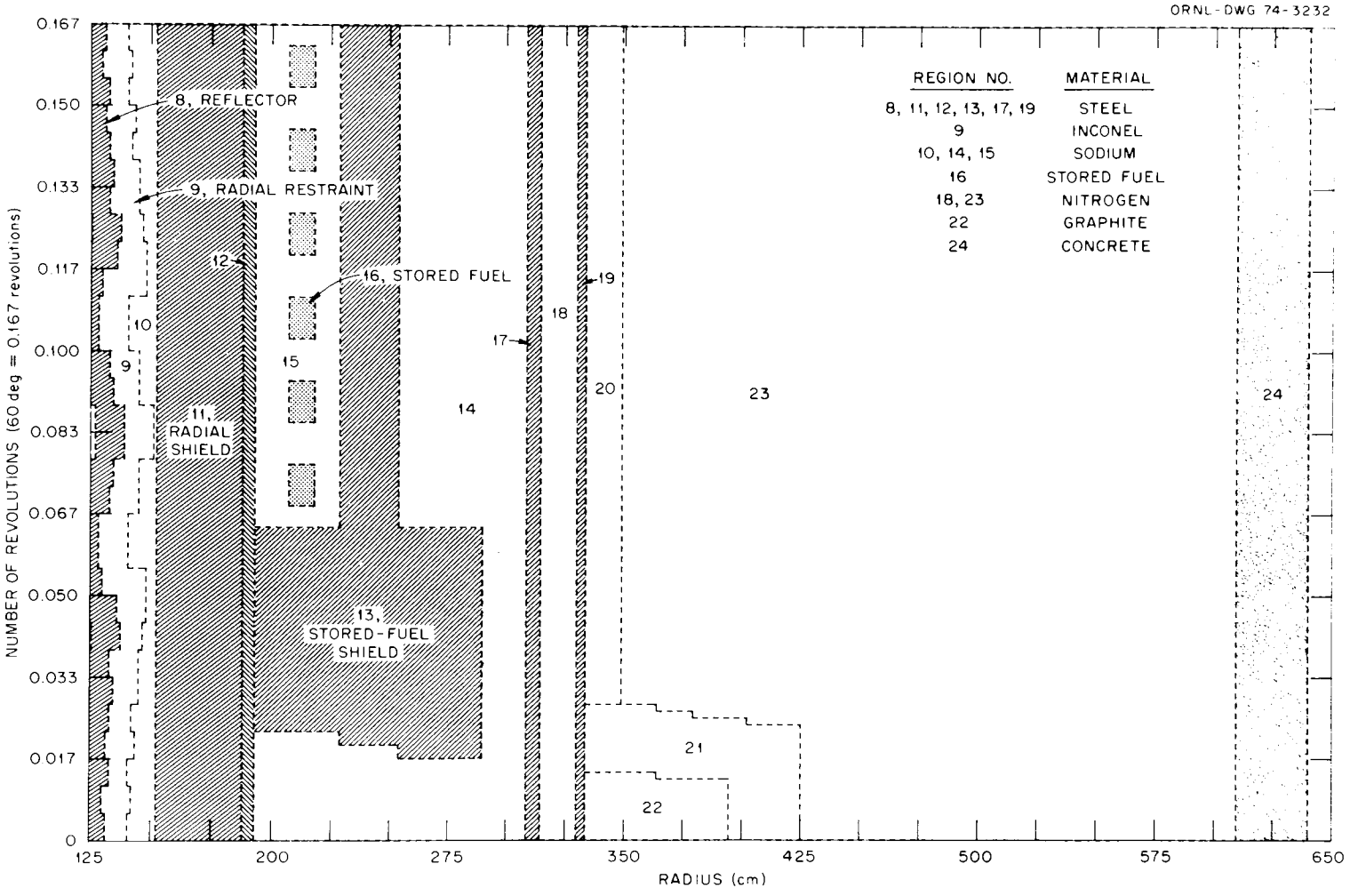

Fig. 2.5. Section of CRBR r,θ Geometry Shown in x,y Geometry. The isoplots given in Figs. 2.6 through 2.9 are given in x,y geometry. Although the theta scale is slightly distorted (compare with geometry given in Fig. 2.4), the values plotted for a given combination of θ and r are accurate.

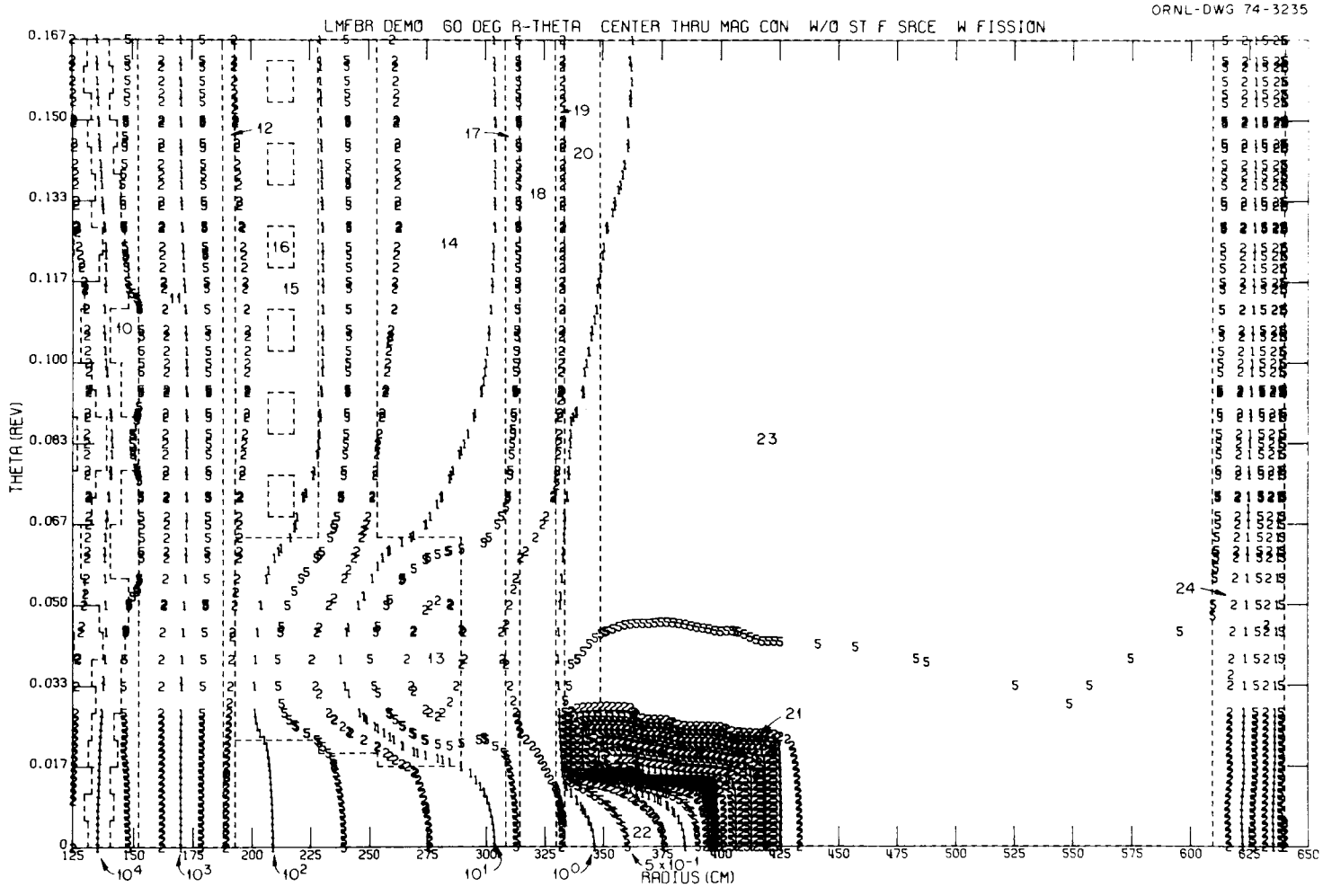

Fig. 2.6. Isoplots of Total Neutron Flux in CRBR System Due to Neutrons from Shutdown Reactor Core (No Neutrons from Stored Fuel). Units are neutrons·cm^{-2}·sec^{-1}.

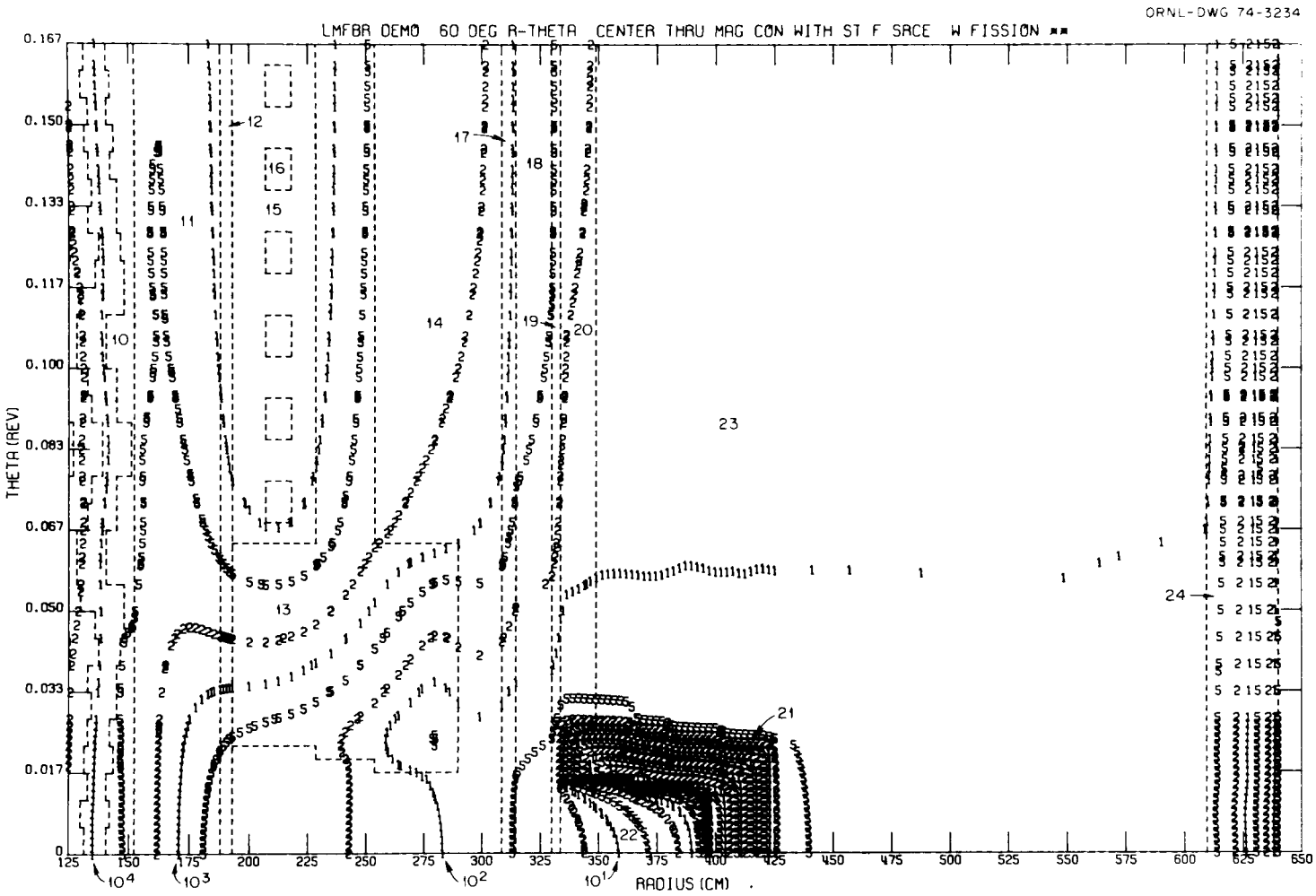

Fig. 2.7. Isoplots of Total Neutron Flux in CRBR System Due to Neutrons from Shutdown Reactor Core and Stored-Fuel Elements. Units are neutrons$\cdot$cm$^{-2}\cdot$sec^{-1}.

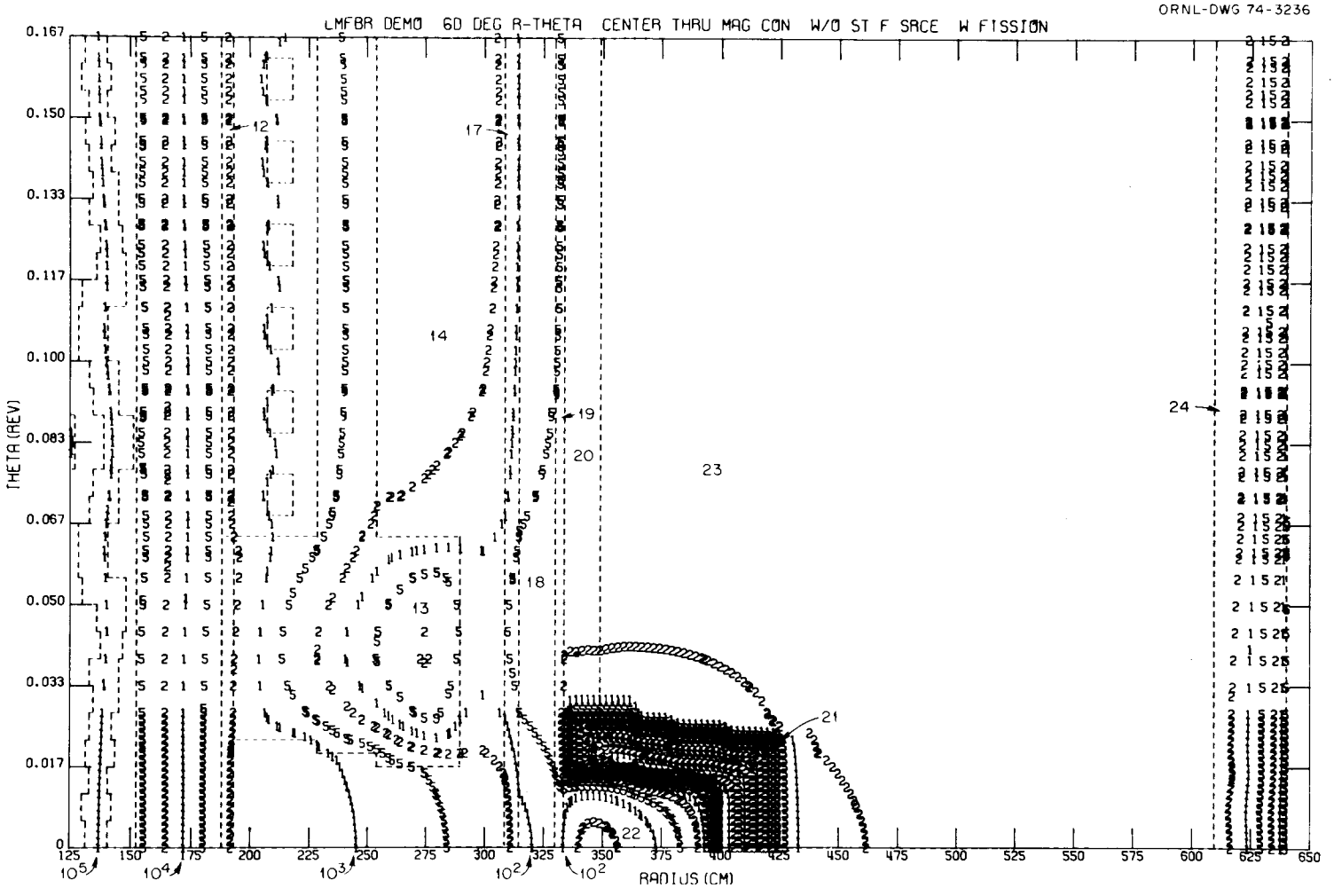

Fig. 2.8. Isoplots of ^{235}U Fission Rates Within CRBR System Due to Neutrons from Shutdown Reactor Core (No Neutrons from Stored Fuel). Plots are of $\sigma_f\phi$, where σ_f is the fission cross section, and ϕ is the neutron flux.

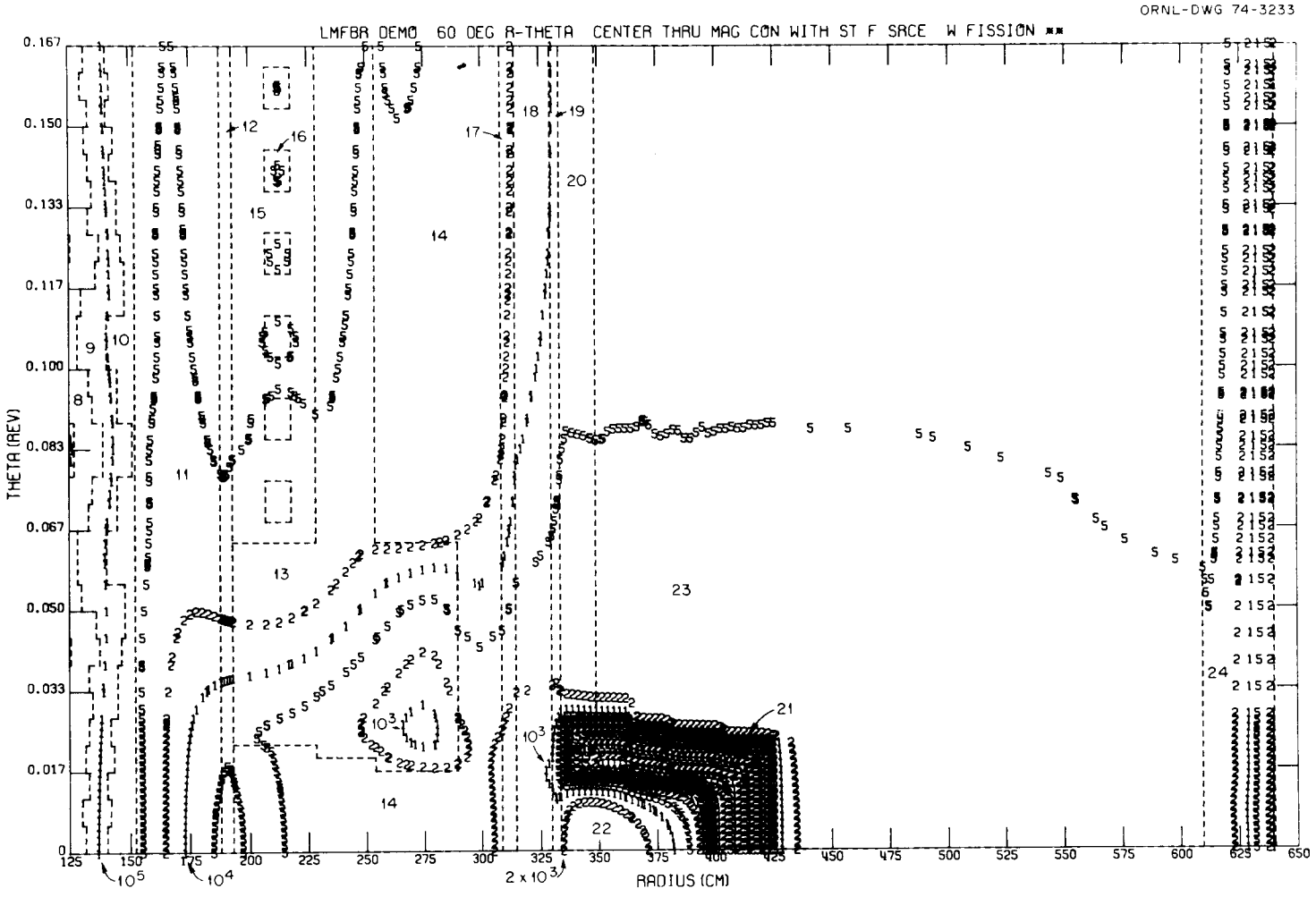

Fig. 2.9. Isoplots of ^{235}U Fission Rates Within CRBR System Due to Neutrons from Shutdown Reactor Core and Stored-Fuel Elements. Plots are of $\sigma_f\phi$, where σ_f is the fission cross section, and ϕ is the neutron flux.

Table 2.10. Comparison of ^{235}U Fission Detector Responses to Core Neutrons and Stored-Fuel Neutrons in CRBR Plant

Case	Reaction Rate[a] (fissions per g of ^{235}U per sec)		Count Rate[b] (counts/sec)		Count Rate Ratio: Core Neutrons / Stored-Fuel Neutrons
	Core Neutrons	Core Plus Stored-Fuel Neutrons	Core Neutrons	Core Plus Stored-Fuel Neutrons	
Reactor at full power; original design (see Fig. 2.1)	5.64(9)[c]	6.15(9)	6.49(10)	7.07(10)	11.6/1
Reactor shut down; original design (see Fig. 2.1)	5.72(-1)	1.02(1)	6.57(0)	1.17(2)	1/16.9
Reactor shut down; B_4C shield added (see Fig. 2.10)	8.46(-2)	1.10(-1)	9.73(-1)	1.27(0)	2.5/1
Reactor shut down; new design (see Fig. 2.11)	5.72(-1)	2.42(0)	6.57(0)	2.78(1)	1/3.2

[a]The reaction rate is equal to the fission rate (such as those given in Figs. 2.8 and 2.9) multiplied by the constant 0.6023/A, where A is the atomic mass (=235 for ^{235}U). The source used was the "start-of-cycle" source (=9.134 x 10^9 neutrons/sec).

[b]The count rate is the reaction rate multiplied by 11.5, which is the total number of grams of ^{235}U in the five detectors. These count rates assume a 100% efficiency of the system. They also assume that each detector is an FFTF intermediate range fission chamber, which actually consists of two fission chambers containing 1.15 g of ^{235}U each.

[c]Read: 5.64 x 10^9.

ORNL-DWG 74-3228

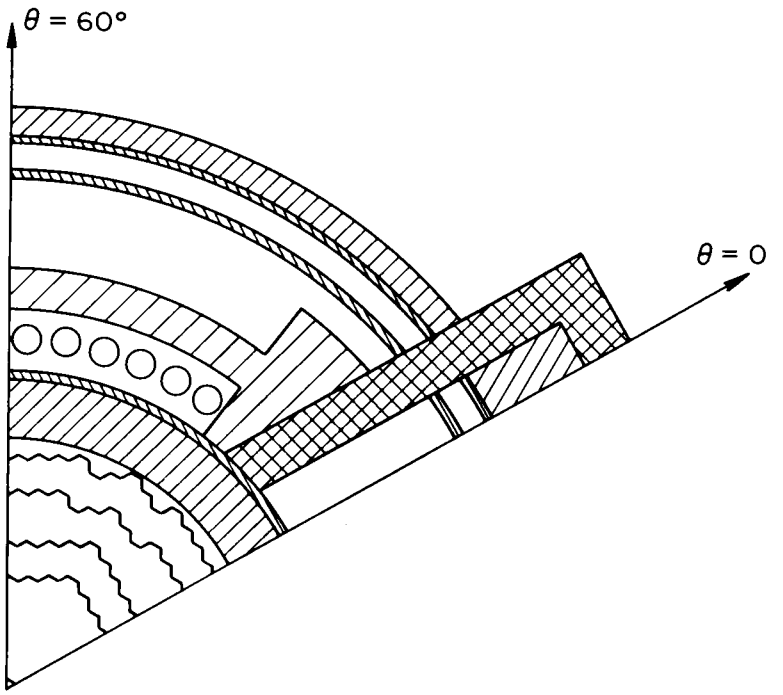

Fig. 2.10. Geometry for r,θ Calculation for CRBR System Having an Extended B_4C Shield.

ORNL-DWG 74-3229R

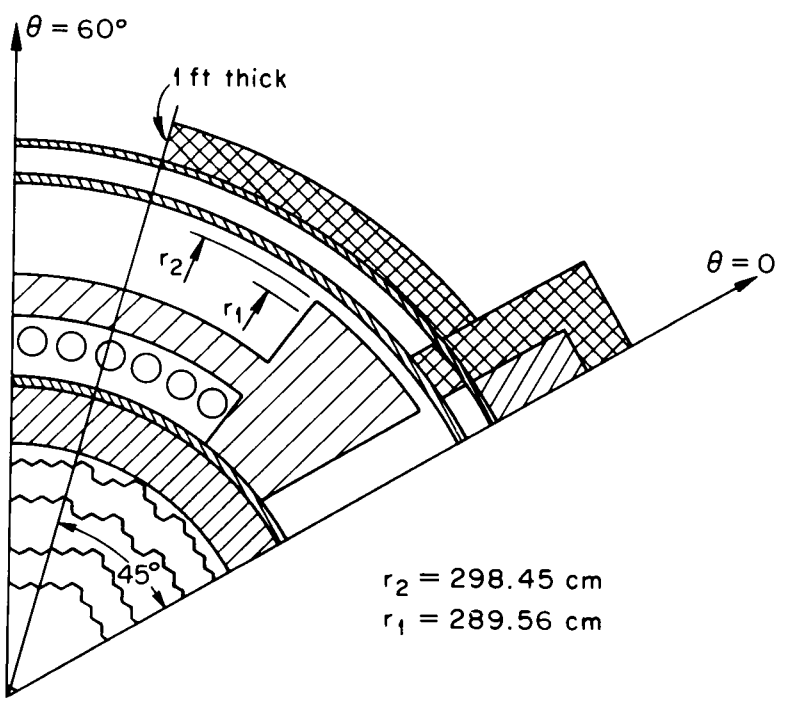

Fig. 2.11. Geometry for r,θ Calculation for CRBR System Having a Revised Stored-Fuel Shield Design.

3. CODE DEVELOPMENT

3.1. Development of DOT IV

Work done by: W. A. Rhoades and D. B. Simpson

Preparatory to the development of the next version of the discrete ordinates code DOT (DOT IV), several two-dimensional discrete ordinates transport codes have been studied with respect to their data storage requirements and the requirements for the transmission of data into and out of the computer memory. A set of reference problems which a new code of this type should be able to solve were designed, and the storage requirements, data transmission, and computation work for these reference problems were evaluated. How the reference problems would fit on several large-scale computers currently available was then examined. It was concluded that the best way to solve very large problems, possibly even those whose data-storage requirements do not exceed the fast memory capacity of existing computers, is to retain one row of information in the fast memory at a given time. That is, blocks of data corresponding to one row each would be successively input, processed, and returned to slow memory or external files. For the reference problems studied, using this procedure in lieu of inputting all the data at one time did not unduly penalize any problem in computer time requirements.

Including a capability for this mode of operation in DOT would offer several advantages, one being that the size of a single-run problem that could be handled would not be limited by the fast memory capacity of the largest computer. With the current versions of DOT, a problem that exceeds the capacity of the fast memory must be divided into a series of runs that are coupled in space and/or energy, which in itself creates difficulties. Another advantage is that DOT could be used effectively to solve fairly large problems on computers having a relatively small fast memory -- such as the CDC-7600 computer. The capability should be made optional, however, so that small problems requiring only a few rows of data that could be stored simultaneously would not be handicapped.

The row option and other features ORNL is planning for DOT-IV were presented to user-representatives from Westinghouse and General Electric at a meeting at AEC-RRD in Washington on October 30. The user-representatives in turn presented their anticipated needs, which had to do mainly with special features rather than with general strategy. General agreement was reached on the developmental approach to be taken.

4. ANALYSIS OF TSF-FTR FIRST-COLLISION STORED-FUEL EXPERIMENT

Work done by: R. L. Childs and F. R. Mynatt

During the month of August an experiment[1] was performed at the Tower Shielding Facility which, together with a successful analysis, will determine the validity of the techniques being used to calculate the ^{239}Pu and ^{235}U fission rates in the FTR stored-fuel modules. In the experiment, the radial regions between the FTR core and a stored-fuel module were mocked up, and the responses of ^{235}U and ^{239}Pu fission detectors just beyond the configurations were interpreted as representing the fission rate at a point in the stored-fuel module. Additional measurements with hydrogen counters and BF_3 detectors yielded information on neutron fluxes at the detector positions.

The first experimental configuration, corresponding to Item I-B in the program plan,[1] is shown in Fig. 4.1. The first region, 4 in. of stainless steel, 6 in. of sodium, and 1 in. of void, is the spectrum modifier. This modifier was designed by Westinghouse ARD to simulate the CRBR core leakage and was thought to provide a reasonably good simulation of the FTR core leakage. The two inconel and two stainless steel slabs behind the spectrum modifier represent the FTR inconel reflector and support structure. The next region mocks up the FTR radial stainless steel shield. This assembly, which was originally designed as an axial shield for an earlier GE demonstration plant experiment, consists of an array of closely packed stainless steel rods in sodium. Details of the radial shield are shown in Fig. 4.2, and the composition of the various materials used throughout the configuration are given in Table 4.1.

Another experimental configuration, corresponding to Item I-D in the program plan,[1] is shown in Fig. 4.2. This configuration more closely resembles the real case in that it mocks up the pool sodium and stainless steel core barrel between the radial shield and the stored fuel.

The analysis of the experiment was begun in September and during this reporting period it consisted of calculations of the fission detector

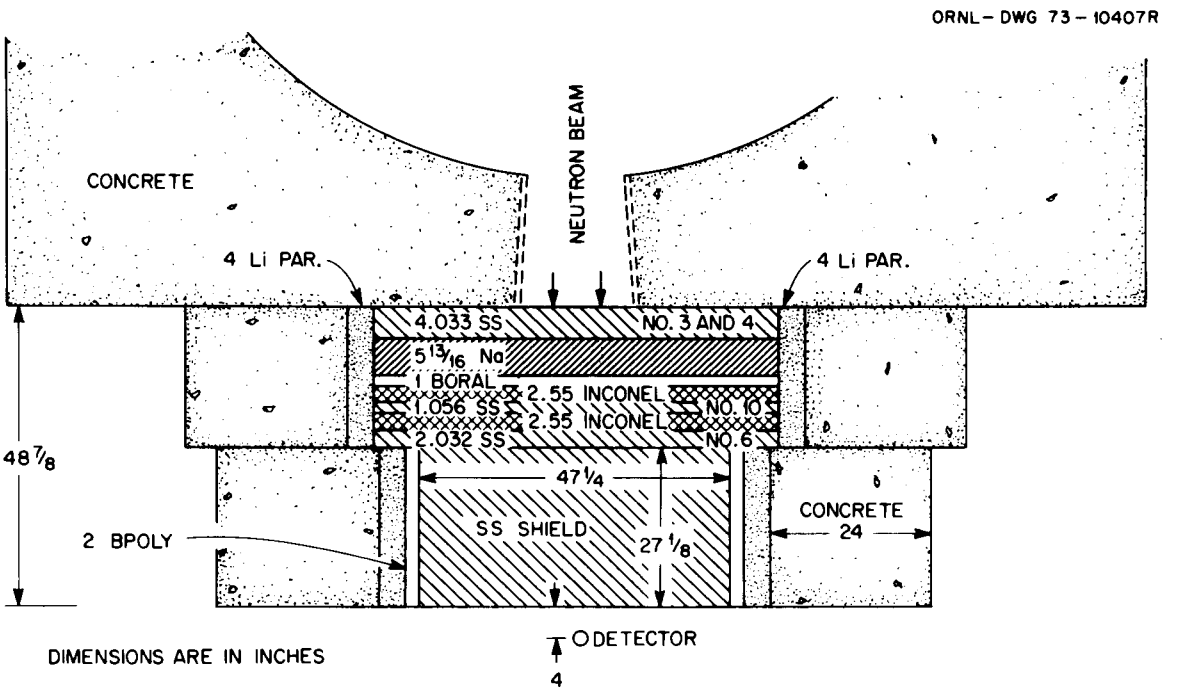

Fig. 4.1. TSF-FTR First-Fission Stored-Fuel Experiment (Item I-B).

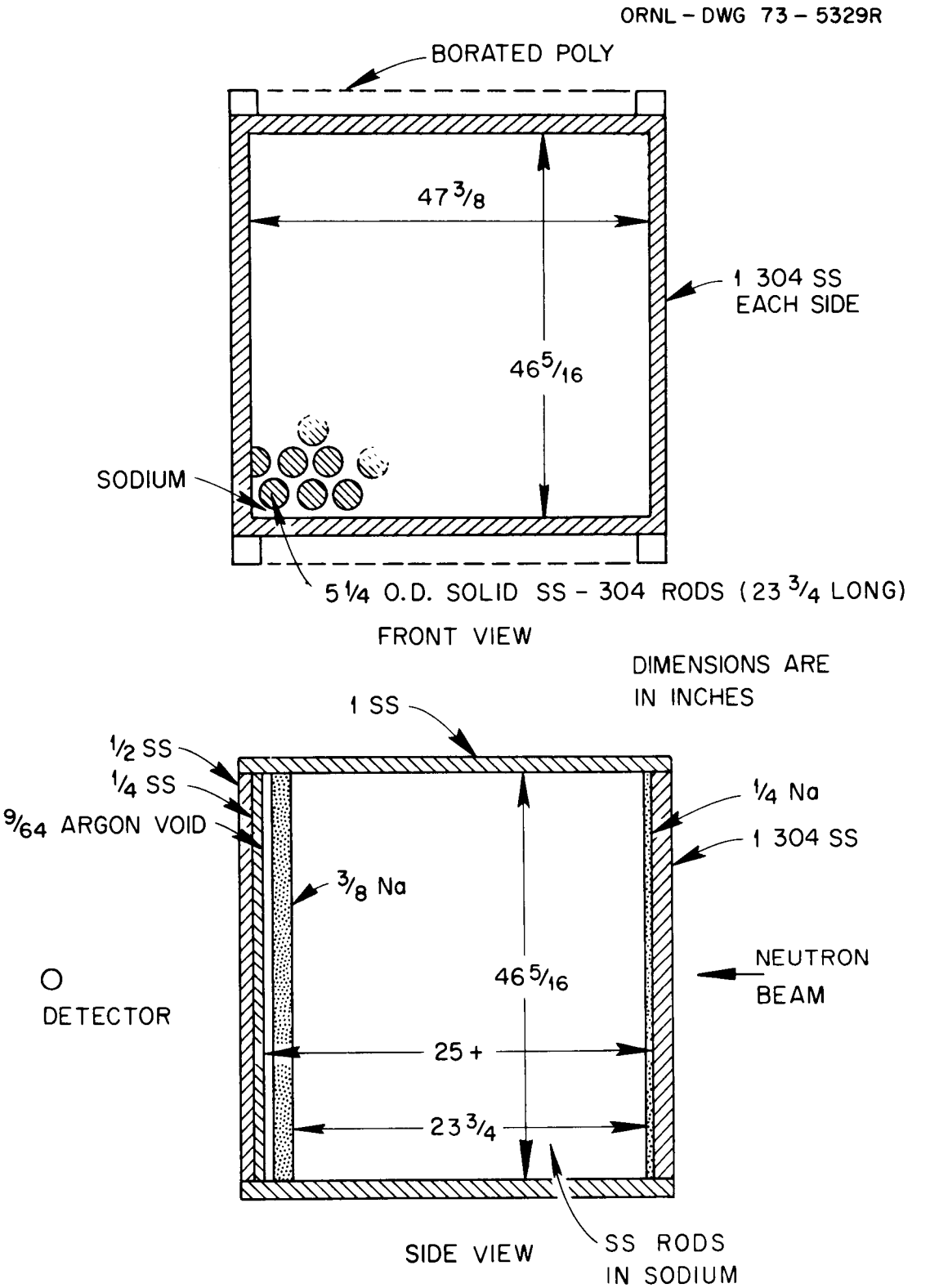

Fig. 4.2. Front and Side View of Stainless Steel Shield Used in TSF-FTR First-Fission Stored-Fuel Experiment.

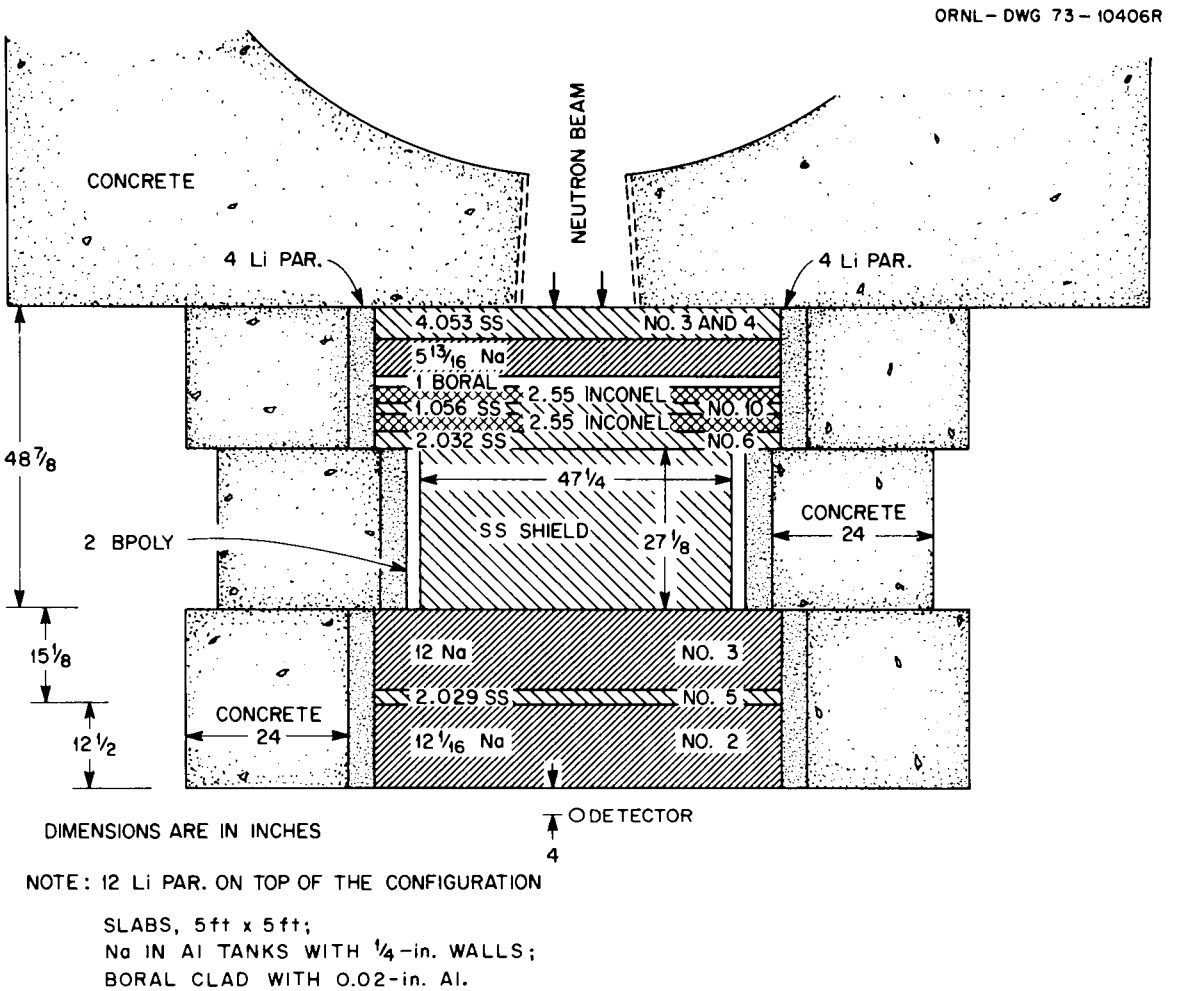

NOTE: 12 Li PAR. ON TOP OF THE CONFIGURATION

SLABS, 5ft x 5ft;
Na IN Al TANKS WITH 1/4-in. WALLS;
BORAL CLAD WITH 0.02-in. Al.

Fig. 4.3. TSF-FTR First-Fission Stored-Fuel Experiment (Item I-D).

Table 4.1. Composition of Materials Used in TSF-FTR First-Fission Stored-Fuel Experiment

Material	Density (g/cc)	Element	wt%	
Aluminum Alloy 6061-T6	2.767	Al	98	
		Mg, Fe, Si	2	
Sodium	0.945	Na	99.7	
		Ca, Zn	0.3	
Boral		B	27.5	
		Al	65.0	
		C	7.5	
			In slabs	In rods
Stainless Steel type 304	7.88	Fe	69.871	72
		Cr	18.46	18.31
		Ni	9.725	8.64
		Mn	1.394	0.90
		Si, C, O	0.55	∿0.68
			Slab No. 1	Slab No. 2
Inconel	8.51	Ni	74.54	74.76
		Cr	15.21	15.72
		Fe	8.63	8.46
		Cu	0.40	0.40
		C	0.098	0.094
		Mn	0.20	0.20
		Co	0.1	0.1
		Mo	0.03	0.03
		Ti	0.09	0.09
		Al	0.10	0.10
		Nb	<0.05	<0.05
			∿99.75	99.31

responses for these two configurations. The calculations were performed in two-dimensional cylindrical geometry with the discrete ordinates code DOT in conjunction with the analytic first-collision computer program GRTUNCL. (GRTUNCL calculates the uncollided flux and the first-collision source resulting from a point source, which is used as input in the DOT code to calculate the flux within the shield.) The air interval between the outer surface of the configuration and the detector was treated in DOT as an extra region in the cylindrical geometry. To obtain the fission counter response, the calculated neutron flux at the detector position was multiplied by the fission cross section for ^{239}Pu or ^{235}U.

The cross sections employed were the 50-group cross sections that have been in general use for the FTR calculations. An S_8 quadrature and P_3 scattering were used throughout.

The resulting calculated detector responses are compared with the experimental responses in Table 4.2. These comparisons show that the calculations are lower than the measurements by a factor of approximately two for the ^{235}U counter and by a factor of about three for the ^{239}Pu counter. After these calculations were performed it was discovered that the ^{239}Pu fission cross sections used were resonance self-shielded cross sections. Since the layer of plutonium is very thin, infinitely dilute cross sections should have been employed. When the ^{239}Pu results are corrected for the self-shielding effect, they, too, are low by a factor of about two.

The reasons for the large discrepancies between the calculated and measured results are not yet understood. Additional work is under way to determine whether the 50 energy groups used in the calculation are adequate.

Table 4.2. Comparison of Calculated and Measured Fission Counter Responses in FTR First-Fission Stored-Fuel Experiment

Configuration[a]	Detector Responses (cpm/MW)			Ratio:	Ratio:
	$^{235}U_{Cd}$	$^{235}U_{Bare}$	$^{239}Pu_{Cd}$	$^{235}U_{Cd}/^{235}U_{Bare}$	$^{235}U_{Cd}/^{239}Pu_{Cd}$
I-B, Calc.	7,538	7,913	1,356	0.9526	5.56
I-B, Exp.	16,600	19,210	4,536	0.8641	3.65
Ratio: Calc./Exp.	0.45	0.41	0.30		
I-D, Calc.	1,800	2,100	330	0.8571	5.45
I-D, Exp.	3,570	4,760	984	0.7500	3.62
Ratio: Calc./Exp.	0.50	0.44	0.34		

[a]See Fig. 4.1 for Configuration I-B and Fig. 4.3 for Configuration I-D.

Section 4. Reference

1. C. E. Clifford *et al.*, "Fast Reactor Experimental Shielding Progress Report for August and September 1973," ORNL-TM-4420, p. 8 (December 1973).

5. ANALYSIS OF TSF INCONEL EXPERIMENT

Work done by: S. Uchida and R. E. Maerker

An analysis of the FTR inconel experiment performed at the ORNL Tower Shielding Facility during July[1] is almost complete, and comparisons of the experimental and calculated data for neutrons are presented here. As pointed out in the previous analytical shielding report,[2] this experiment was performed both to study the radiation-attenuating properties of the FTR reflector material and to provide an experimental test for calculated quantities based on nickel cross sections, which are not well known.

In the experiment the radiation source was a beam from the Tower Shielding Reactor (TSR-II) filtered through the Westinghouse Spectrum Modifier (4 in. of stainless steel, 6 in. of sodium, and 1 in. of boral).[3] Each of the two inconel configurations tested, one 2-1/2 in. thick and the other 5 in. thick, was positioned adjacent to the spectrum modifier as shown in Figs. 5.1 and 5.2. Measurements made at various locations behind the configurations included neutron spectral measurements with the NE-213 spectrometer and hydrogen counters, integral neutron flux measurements with Bonner balls, and gamma-ray spectral measurements with a sodium iodide spectrometer.

In the analysis the two-dimensional discrete ordinates code DOT in conjunction with the analytic first-collision code GRTUNCL and the analytic first-collision code FALSTF has been used to calculate the transport through the configurations mocked up in cylindrical geometry. The calculations used 21 neutron groups, 18 gamma-ray groups, P_3 scattering, and an S_8 quadrature. The composition used for the inconel was the same as the measured composition.

The calculated neutron count rates for Bonner balls located on the beam center line 24 in. behind the configuration are compared with the experimental count rates in Table 5.1. In all cases the calculated count rates are higher than the measured count rates. The fact that the

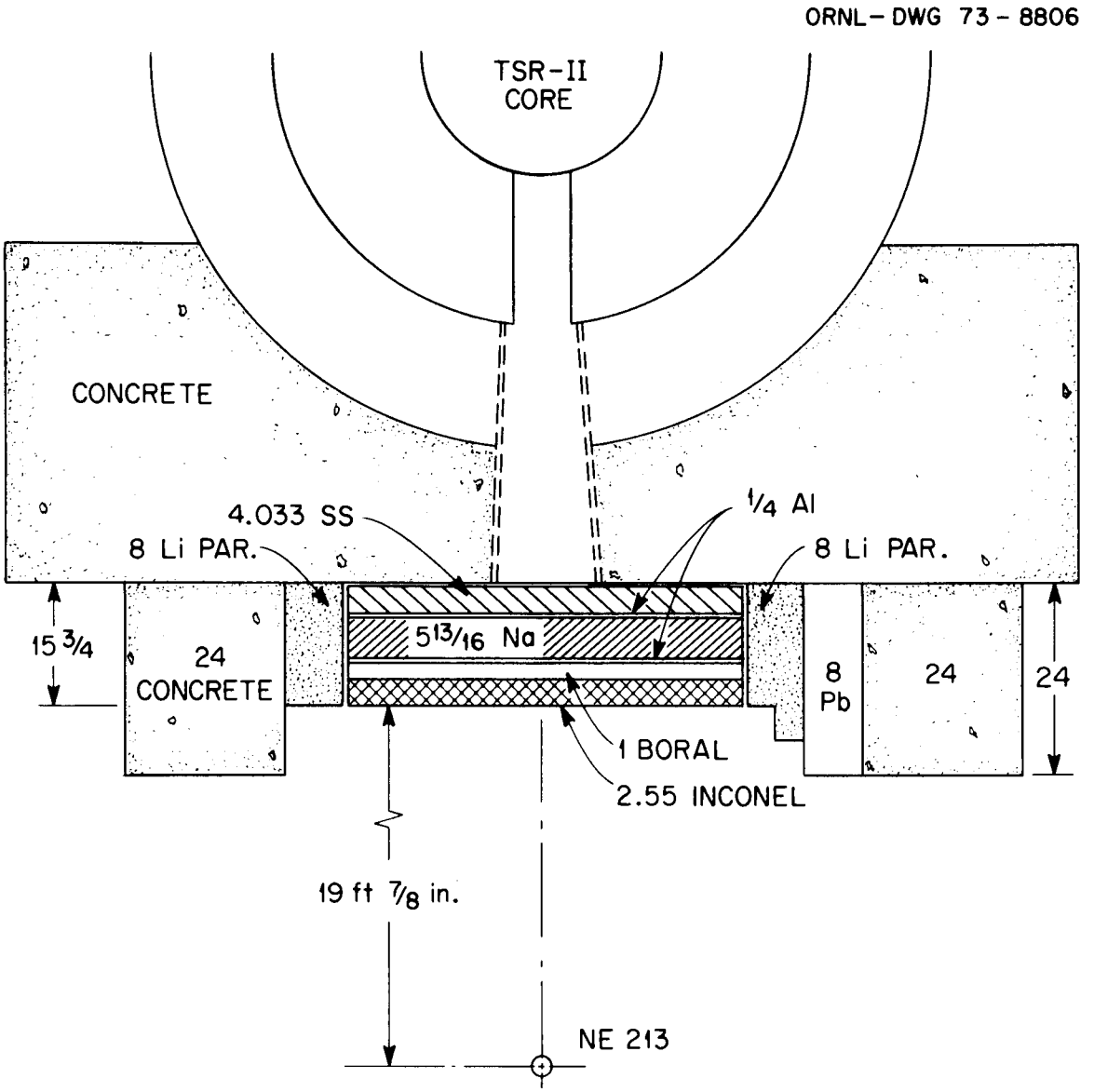

DIMENSIONS ARE IN INCHES EXCEPT AS NOTED

NOTE : MINIMUM OF 8-in. Li PAR. ON TOP OF CONFIGURATION

Fig. 5.1. Experimental Configuration for Spectrum Modifier Plus 2-½-in. Inconel, Item A.

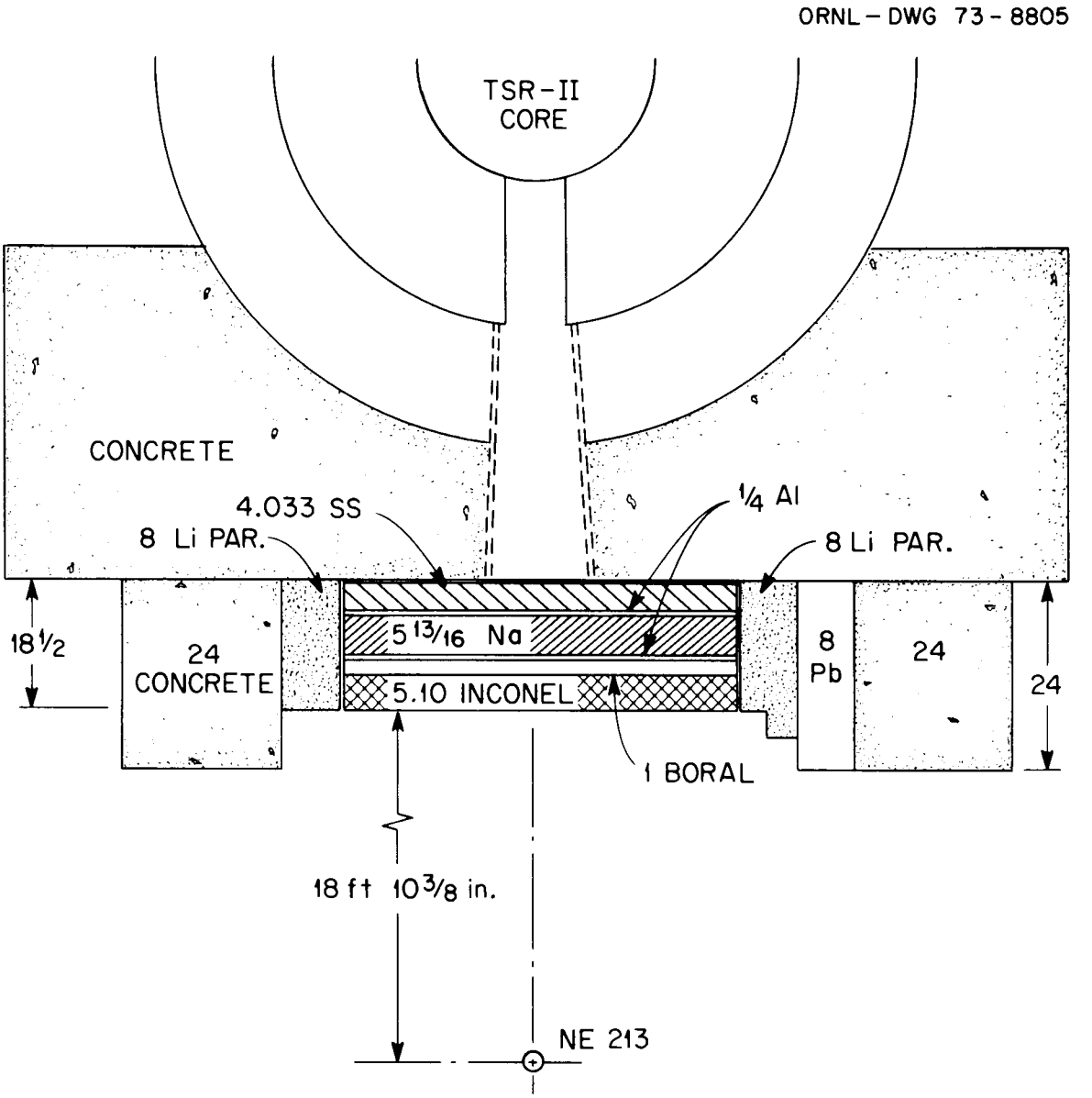

DIMENSIONS ARE IN INCHES EXCEPT AS NOTED

NOTE: MINIMUM OF 8-in. Li PAR. ON TOP OF CONFIGURATION

Fig. 5.2. Experimental Configuration for Spectrum Modifier Plus 5-in. Inconel, Item B.

Table 5.1. Comparison of DOT-Calculated and Measured (Bonner Ball) Neutron Count Rates on Center Line 24 in. Behind Inconel Configurations

(Westinghouse Spectrum Modifier Precedes Inconel)

	Count Rate (cpm/kW)		
	3-in. Ball	6-in. Ball	10-in. Ball
24 in. Behind Spectrum Modifier (No Inconel)[a]			
Calculated, scattered	6.39(5)[b]	4.44(6)	2.54(6)
Calculated, uncollided	2.3(4)	5.63(5)	6.04(5)
Calculated, total	6.62(5)	5.00(6)	3.14(6)
Measured	5.27(5)	4.59(6)	2.95(6)
Ratio: Calc./Meas.	1.26	1.09	1.07
24 in. Behind 2.55 in. of Inconel (Item A.3)[c]			
Calculated, scattered	3.90(5)	2.68(6)	1.40(6)
Calculated, uncollided	2.68(3)	7.57(4)	8.31(4)
Calculated, total	3.93(5)	2.76(6)	1.48(6)
Measured	2.87(5)	2.27(6)	1.23(6)
Ratio: Calc./Meas.	1.37	1.22	1.20
24 in. Behind 5.10 in. of Inconel (Item B.3)[c]			
Calculated, scattered	2.66(5)	1.61(6)	7.53(5)
Calculated, uncollided	3.50(2)	1.03(4)	1.14(4)
Calculated, total	2.66(5)	1.62(6)	7.64(5)
Measured	2.11(5)	1.45(6)	6.98(5)
Ratio: Calc./Meas.	1.26	1.12	1.09

[a]Taken from earlier calculation (ORNL-TM-4402, p. 60).

[b]Read: 6.39×10^5.

[c]Item number corresponds to outline of experiment given in ORNL-TM-4364, p. 1.

difference is greater for the thinner configuration is an anomaly not yet explainable.

Comparisons of the experimental and calculated results in the energy range of the hydrogen counter ($\sim$ 0.05 to 1.4 MeV) at a point 12 in. behind the configurations are presented in Table 5.2 and Fig. 5.3. Again, most of the calculated quantities (in this case energy fluxes) are higher than the measured quantities and again agreement is better for the 5-in. configuration than for the 2-1/2-in. configuration.

For the higher energy ranges, those covered by the NE-213 spectrometer, the calculated neutron fluxes are lower than the measured fluxes for a detector position approximately 19 ft beyond the configurations (see Table 5.3 and Fig. 5.4). Also, in this case the agreement is better for the 2-1/2-in. configuration than for the 5-in. configuration.

As pointed out above, this analysis gives results that are in better agreement with the thick-slab experimental data than with the thin-slab data in some energy regions; also it gives results that are higher than the experimental data in some energy regions and lower than the data in other energy regions. At this point, we can only guess that compensating errors are occurring in the calculations and that they can be traced to the nickel cross sections.

Section 5 References

1. C. E. Clifford *et al.*, "Fast Reactor Experimental Shielding Monthly Progress Report for July 1973," ORNL-TM-4364 (September 1973).

2. F. R. Mynatt *et al.*, "Fast Reactor Analytical Shielding Progress Report for July and August," ORNL-4402, p. 73 (November 1973).

3. ORNL-TM-4402, op. cit., p. 56.

Table 5.2. Comparison of DOT-Calculated and Measured (Hydrogen Counter) Neutron Fluxes 12 in. Behind Inconel Configurations[a]

(Westinghouse Spectrum Modifier Precedes Inconel)

Group No.	Energy Interval (MeV)	Neutron Flux (neutrons·cm^{-2}·min^{-1}·W^{-1}) Calculated Uncollided	Scattered	Total	Measured	Ratio: Calc. Flux / Meas. Flux
	12 in. Behind Spectrum Modifier (No Inconel)[b]					
7	0.907-1.35	7.8(1)[c]	6.42(2)	7.20(2)	6.79(2)	1.06
8	0.550-0.907	4.1(1)	8.12(2)	8.54(2)	7.73(2)	1.10
9	0.334-0.550	2.6(1)	9.59(2)	9.84(2)	8.61(2)	1.14
10	0.202-0.334	2.4(1)	7.74(2)	7.99(2)	7.76(2)	1.03
11	0.123-0.202	9.0(0)	6.93(2)	7.02(2)	9.47(2)	0.74
12	0.0409-0.123	7.0(0)	7.54(2)	7.61(2)	1.18(3)[d]	0.64[d]
7-12	0.0409-1.35	1.85(2)	4.63(3)	4.82(3)	5.22(3)	0.92
	12 in. Behind 2.55 in. of Inconel (Item A.2a)[e]					
6	1.35-2.02	2.22(1)	2.82(2)	3.04(2)	f	f
7	0.907-1.35	1.17(1)	4.06(2)	4.18(2)	3.87(2)	1.08
8	0.550-0.907	6.54(0)	5.93(2)	6.00(2)	5.03(2)	1.19
9	0.334-0.550	2.75(0)	5.54(2)	5.57(2)	4.52(2)	1.23
10	0.202-0.334	1.60(0)	5.15(2)	5.17(2)	4.49(2)	1.15
11	0.123-0.202	5.57(-1)	5.42(2)	5.43(2)	4.00(2)	1.36
12	0.0491-0.123[g]	1.68(-1)	5.39(2)	5.39(2)	4.29(2)	1.26
7-12	0.0491-1.35	2.33(1)	3.15(3)	3.17(3)	2.62(3)	1.21
	12 in. Behind 5.10 in. of Inconel (Item A.2b)[e]					
6	1.35-2.02	3.12(0)	1.05(2)	1.08(2)	f	f
7	0.907-1.35	1.72(0)	2.12(2)	2.14(2)	2.18(2)	0.98
8	0.550-0.907	1.01(0)	3.76(2)	3.77(2)	3.39(2)	1.11
9	0.334-0.550	2.79(-1)	2.97(2)	2.97(2)	3.11(2)	0.95
10	0.202-0.334	1.02(-1)	3.06(2)	3.06(2)	3.01(2)	1.02
11	0.123-0.202	3.25(-2)	3.58(2)	3.58(2)	3.10(2)	1.15
12	0.0409-0.123	4.83(-3)	4.46(2)	4.46(2)	3.38(2)	1.32
					3.79(2)[a]	1.18
13	0.0117-0.040	1.14(-6)	4.99(1)	4.99(1)	8.78(1)[a]	0.57
7-13	0.0117-1.35	3.15(0)	2.05(3)	2.05(3)	1.93(3)	1.06

[a]Measurements identified with superscript a were made with double-parameter hydrogen counter; all other measurements were made with single-parameter hydrogen counter.

[b]Taken from earlier calculation (ORNL-TM-4402, p. 60).

[c]Read: 7.8×10^1.

[d]Gamma-ray contamination is probably present.

[e]Item number corresponds to outline of experiment given in ORNL-TM-4364, p. 1.

[f]Measured intensity too weak to be reliable.

[g]The width of energy interval No. 12 is smaller for this configuration.

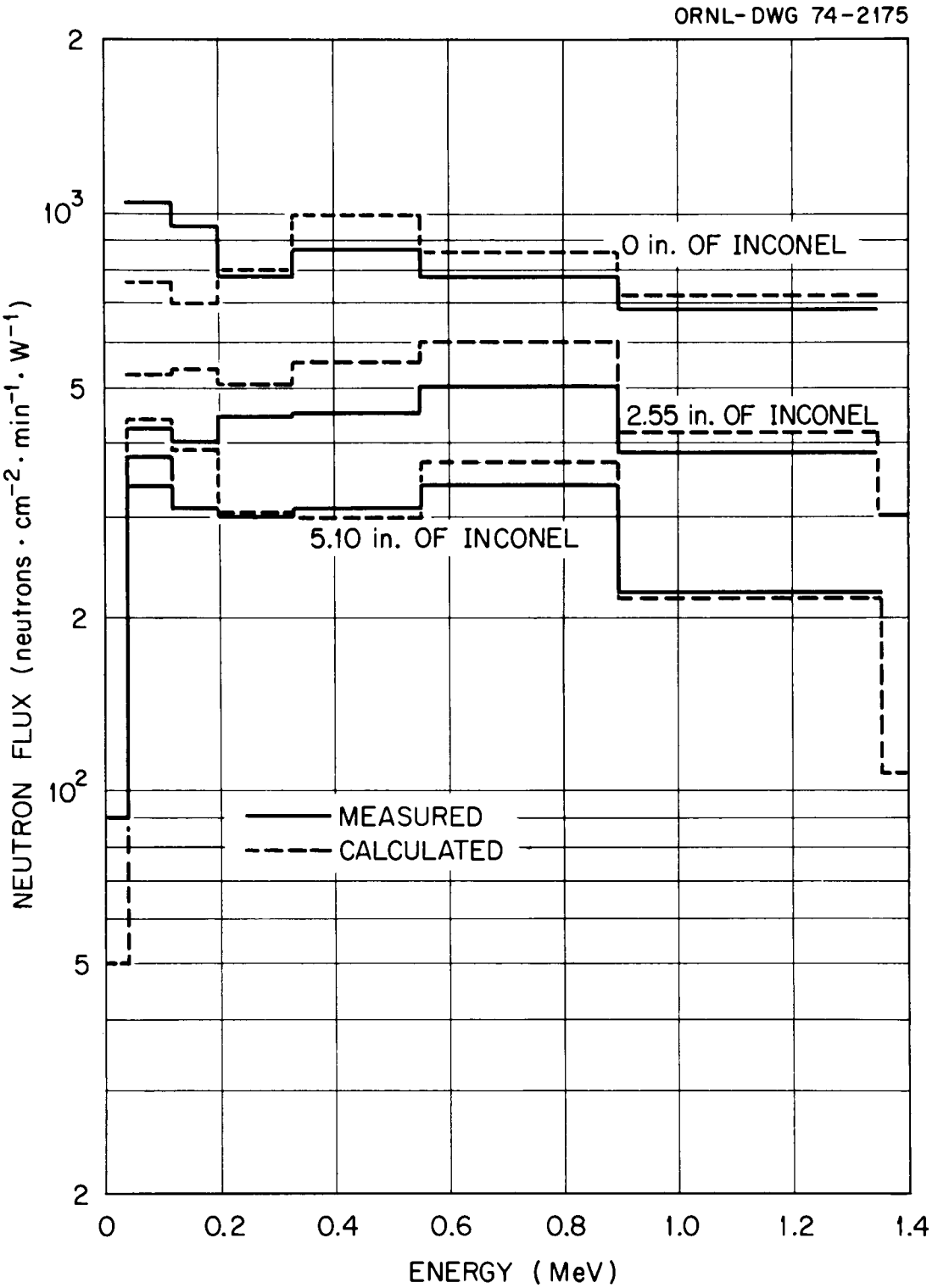

Fig. 5.3. Comparison of DOT-Calculated and Measured (Hydrogen Counter) Neutron Fluxes 12 in. Behind Inconel Configurations. Inconel preceded by Westinghouse Spectrum Modifier.

Table 5.3. Comparison of DOT-Calculated and Measured (NE-213) Neutron Fluxes ∿ 19 ft Behind Inconel Configurations[a]

(Westinghouse Spectrum Modifier Precedes Inconel)

Group No.	Energy Interval (MeV)	Neutron Flux (neutrons·cm^{-2}·min^{-1}·W^{-1}) Calculated Uncollided	Scattered	Total	Measured	Ratio: Calc. Flux / Meas. Flux
	19 ft 7/8 in. Behind 2.55 in. of Inconel (Items A.1 and A2b)[b]					
1	10-15	7.91(-2)[c]	3.95(-2)	1.19(-1)	d	d
2	6.7-10	3.19(-1)	1.92(-1)	5.10(-1)	5.75(-1)	0.89
3	4.49-6.7	6.78(-1)	4.57(-1)	1.14(0)	1.25(0)	0.91
4	3.01-4.49	1.24(0)	7.37(-1)	1.98(0)	2.01(0)	0.99
5	2.02-3.01	1.65(0)	1.36(0)	3.01(0)	3.35(0)	0.90
6	1.35-2.02	1.77(0)	2.07(0)	3.84(0)	4.16(0)	0.92
7	0.907-1.35	9.34(-1)	2.84(0)	3.77(0)	4.27(0)	0.89
					3.98(0)[a]	0.95
8	0.55-0.907	5.21(-1)	4.18(0)	4.70(0)	4.57(0)[a]	1.03
2-8	0.55-10	7.11(0)	1.18(1)	1.89(1)	2.0(1)	0.95
	18 ft 10 3/8 in. Behind 5.10 in. of Inconel (Items B1 and B.2b)[b]					
1	10-15	1.46(-2)	1.28(-2)	2.74(-2)	d	d
2	6.7-10	4.26(-2)	5.63(-2)	9.89(-2)	1.29(-1)	0.77
3	4.49-6.7	8.05(-2)	1.20(-1)	2.01(-1)	2.45(-1)	0.82
4	3.01-4.49	1.66(-1)	1.96(-1)	3.62(-1)	4.14(-1)	0.87
5	2.02-3.01	2.49(-1)	4.44(-1)	6.93(-1)	8.83(-1)	0.78
6	1.35-2.02	2.62(-1)	8.11(-1)	1.07(0)	1.28(0)	0.84
7	0.907-1.35	1.45(-1)	1.56(0)	1.71(0)	1.80(0)	0.95
					2.07(0)[a]	0.83
8	0.55-0.907	8.49(-2)	2.81(0)	2.90(0)	2.97(0)[a]	0.98
2-8	0.55-10	1.03(0)	6.00(0)	7.04(0)	7.86(0)	0.90

[a]Measurements identified with superscript a were made with 10-atm hydrogen counter; all other measurements were made with NE-213 spectrometer.

[b]Item number corresponds to outline of experiment given in ORNL-TM-4364, p. 1.

[c]Read: 7.91×10^{-2}.

[d]Measured intensity too weak to be reliable.

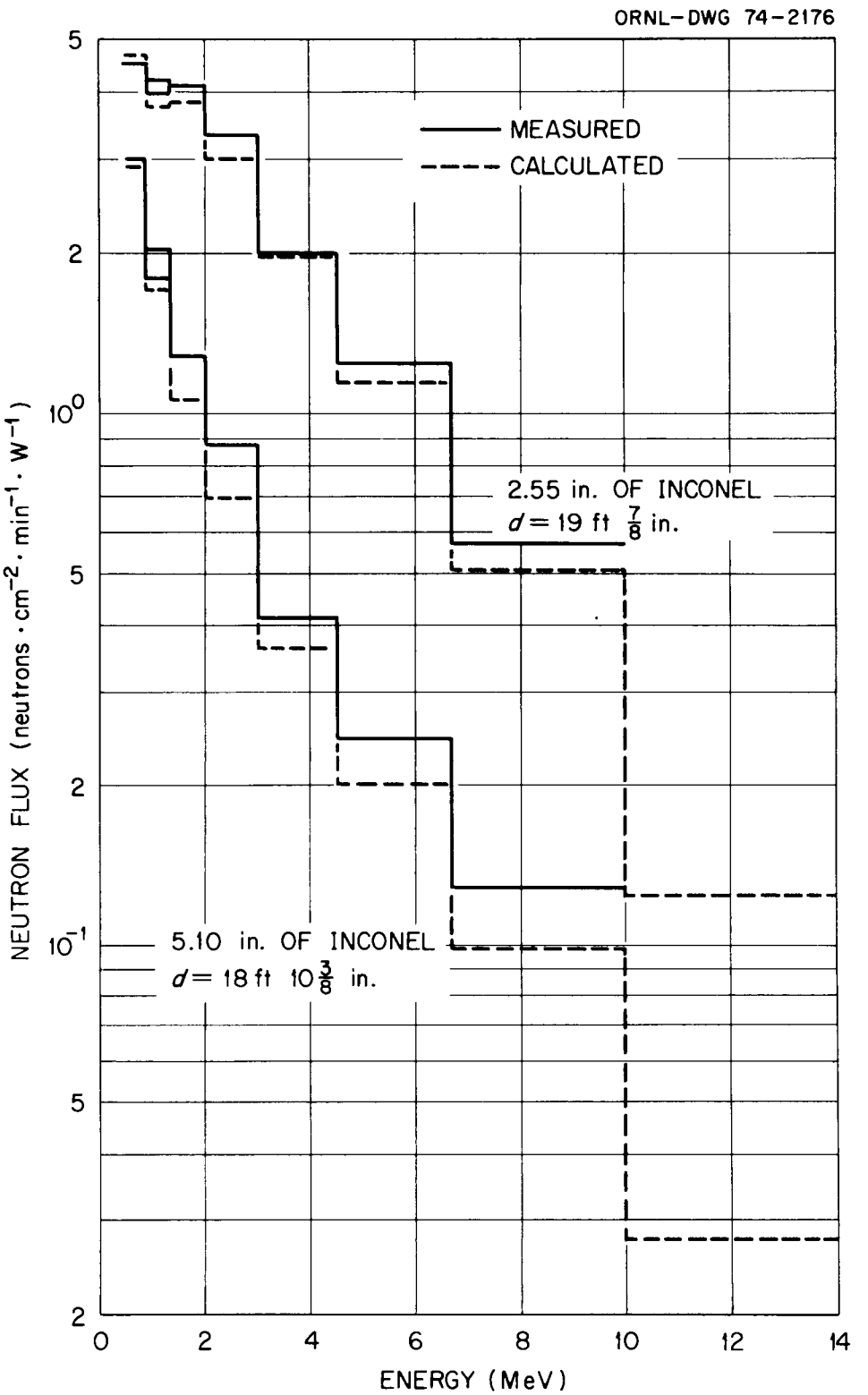

Fig. 5.4. Comparison of DOT-Calculated and Measured (NE-213) Neutron Fluxes Behind Inconel Configurations. Inconel preceded by Westinghouse Spectrum Modifier.

6. CALCULATIONS OF GAMMA-RAY HEATING IN IRON: ANALYSIS OF TSF MEASUREMENTS WITH THERMOLUMINESCENT DOSIMETERS (TLD's)

Work done by: F. B. K. Kam

The reliability of thermoluminescent dosimeters ($CaSO_4$:Dy or CaF_2:Dy powder in iron capsules) for measuring gamma-ray heating continues to be of concern. It was reported previously[1] that ANISN calculations of the energy deposition by ^{60}Co gamma rays in iron yielded results that were 15 to 30% lower than those measured with the TLD's in a specially designed Tower Shielding experiment.[2] In that experiment both the ^{60}Co source and the TLD's were embedded in iron.

In an attempt to investigate the discrepancy, a new experiment[3] and accompanying calculations were performed for a configuration in which the ^{60}Co source was again embedded in iron but the TLD's were placed at 1-in. intervals on the surface of the iron as shown in Figs. 6.1 and 6.2. So that the calculational method could be tested against measurements made with another detector, the experiment also included measurements with an NaI spectrometer at four angles from the Z axis.

The analysis of the TLD measurements was performed with the DOT and ANISN discrete ordinates codes in cylindrical and spherical geometry respectively. Both calculations used the same AMPX-prepared 30-group gamma-ray cross sections employed in the earlier analysis. A point-kernel calculation was also performed.

In the cylindrical geometry assumed for the first DOT calculation, the cylinder height and radius were taken to be 22.70 cm and 91.44 cm, respectively, with the source located in a void region in the center of the cylinder. It was found that the region beyond a radius of 44 cm did not contribute significantly and could be eliminated from the calculation; therefore, for the final calculation the radius of the cylinder was reduced to 44 cm. In addition, the cylinder was assumed to be symmetrical about the plane containing the source, which allowed the region above the source to be treated as a reflection plane. By thus reducing the amount of

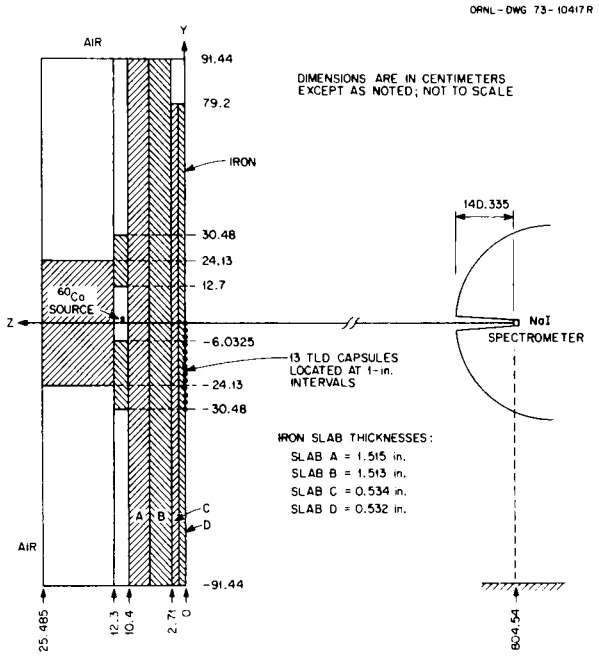

Fig. 6.1. Y-Z Plane of Configuration for ^{60}Co Gamma-Ray Experiment.

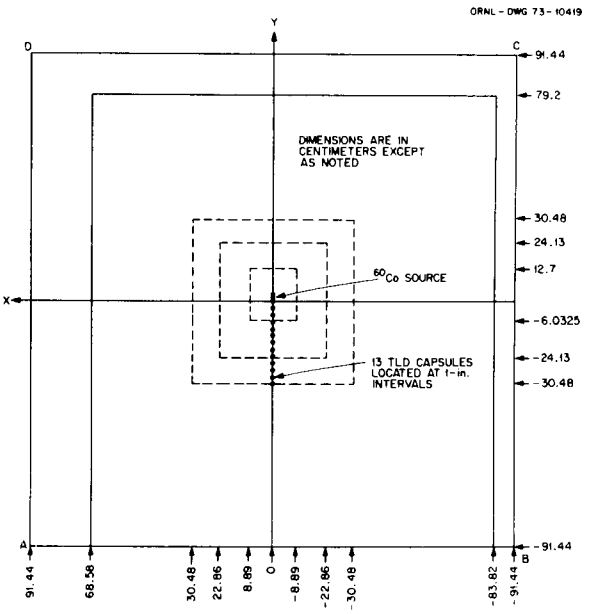

Fig. 6.2. X-Y Plane of Configuration for ^{60}Co Gamma-Ray Experiment.

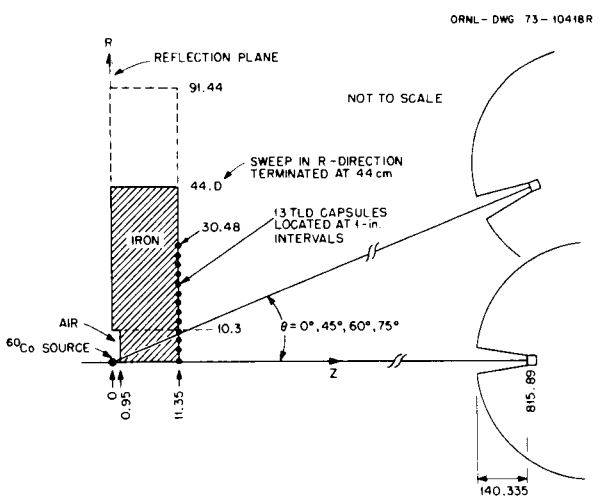

Fig. 6.3. R-Z Geometry for DOT Calculations of Gamma-Ray Energy Deposition and for DOT-FALSTF Calculations of Gamma-Ray Spectra.

volume to be included in the calculation, that part remaining could be treated in greater spatial detail. The resulting geometry is shown in Fig. 6.3, in which z, the cylinder axis, corresponds to the experimental axis of symmetry (see Fig. 6.1). The cylinder radius R corresponds to Y in the experimental configuration.

It is to be noted that the radial dimensions for the void in the center of the calculational model differ from those of the experiment. This is partially because in the calculations the source is centered in the void, whereas in the experiment it is not. Also, in the calculations it was necessary to select a radius for the cylindrical void that would result in the void having the same volume as that of the rectangularly shaped void in the experiments.

The energy deposition was obtained from the DOT calculations for the points indicated on the flat surface of the cylinder. The results are compared with the TLD measurements (those corrected for spectral dependence by the 1/f factor) in Fig. 6.4 and in Table 6.1. The slant iron thicknesses shown include the 1/8-in. wall thickness of the capsule in the TLD. That is, the first entry in the table is for the TLD on the cylinder axis, for which the slant iron thickness is listed as 10.716 cm. This includes 10.4 cm of iron in the configuration and 0.316 cm of iron in the capsule.

The DOT calculations and measurements agree to within $\pm 20\%$ for radial distances out to 7 in. (iron thicknesses of about 19 cm), but beyond 7 in. the measurements are systematically higher, which seems to be characteristic of the TLD measurements when the total exposure of the dosimeter is low (in this case less than about 0.1 r). As pointed out in an earlier progress report,[2] this may be due to the methods of handling the experimental and readout backgrounds, and these effects are currently under investigation.

The ANISN calculations were performed for a spherical model consisting of the source centered in a central void and successive concentric spheres of iron with thicknesses corresponding to the slant ranges used for the

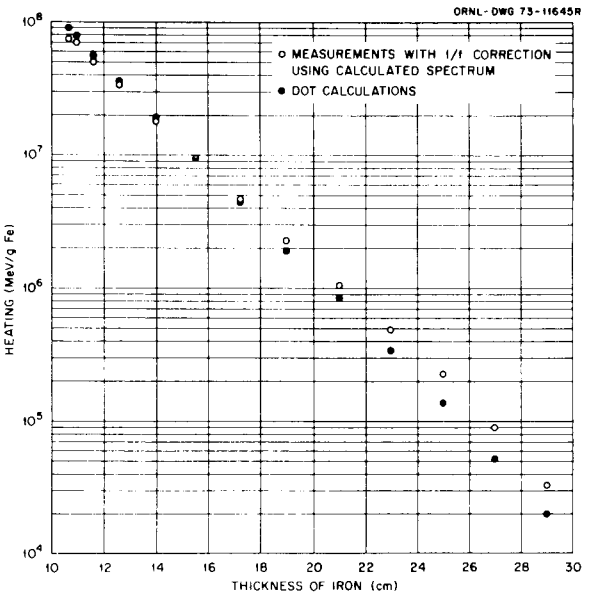

Fig. 6.4. Comparison of DOT-Calculated and Measured TLD Energy Deposition Due to ^{60}Co Gamma Rays Penetrating to Surface of Iron Slab.

Table 6.1. Comparison of Measured and Calculated TLD Energy Deposition Due to ^{60}Co Gamma Rays Penetrating to Surface of Iron Slab

TLD Radial Position (in.)	Slant Iron Thickness (cm)	TLD Exposure (r)	Energy Deposition (MeV/g·Fe)				
			Uncorrected TLD	1/f x TLD	DOT	ANISN	Point Kernel
0	10.716	1.30240	6.64(7)[a]	7.44(7)	9.00(7)	9.00(7)	9.78(7)
1	10.950	1.20480	6.14(7)	6.88(7)	7.85(7)	7.90(7)	8.74(7)
2	11.627	0.88480	4.51(7)	5.05(7)	5.60(7)	5.70(7)	6.23(7)
3	12.674	0.57600	2.94(7)	3.32(7)	3.50(7)	3.50(7)	3.71(7)
4	14.009	0.30880	1.57(7)	1.77(7)	1.90(7)	1.85(7)	1.95(7)
5	15.558	0.16320	8.32(6)	9.48(6)	9.35(6)	8.70(6)	8.27(6)
6	17.265	0.08048	4.10(6)	4.67(6)	4.40(6)	4.00(6)	4.29(6)
7	19.085	0.03936	2.01(6)	2.29(6)	1.90(6)	1.70(6)	1.86(6)
8	20.990	0.01792	9.14(5)	1.05(6)	8.30(5)	7.40(5)	7.83(5)
9	22.958	0.00833	4.25(5)	4.89(5)	3.35(5)	2.95(5)	3.23(5)
10	24.976	0.00382	1.95(5)	2.24(5)	1.35(5)	1.12(5)	1.34(5)
11	27.031	0.00151	7.72(4)	8.88(4)	5.10(4)	4.60(4)	5.39(4)
12	29.116	0.00056	2.85(4)	3.28(4)	1.95(4)	1.80(4)	2.15(4)

[a]Read as: 6.64×10^7.

DOT calculations. Since in these calculations the TLD positions were assumed to be embedded in the iron, it was necessary to correct for backscattering in the iron. The results, included in Table 6.1, are very similar to those obtained with DOT.

The point kernel results, also included in the table, are higher than those from the DOT and ANISN calculations. This is to be expected since the point kernel technique used gamma-ray buildup factors for an infinite iron medium and the effect of backscattering is retained. Thus the point-kernel calculations are conservative.

In order to ensure ourselves that the persistent discrepancies between the measurements and the calculations are not due to consistent errors in the calculational methods, the calculations were extended to calculate the spectra of gamma rays at the four locations of the NaI spectrometer (see Figs. 6.1 and 6.3). The flux at these points outside the shield were calculated with the FALSTF code which uses the flux calculated by DOT for points inside the shield to determine the last-flight contribution of all sources to a point outside the shield. (A special version of FALSTF which corrected for the reflection plane was required for these calculations.)

The calculated and measured gamma-ray spectra at the four spectrometer positions are compared in Figs. 6.5 and 6.6. The calculated fluxes are also given in Table 6.2. Good agreement exists between the measurements and calculations for the emergent angles of 0, 45, and 60 deg; however, for the emergent angle of 75 deg, the measured spectrum is significantly higher than the calculated spectrum below 0.8 MeV. The higher experimental values are probably due to gamma rays penetrating the thin regions of the shield on the back side and scattering to the spectrometer.

The integrals of the energy spectra for each of the four angles are as follows:

Angle (deg)	Measured Integral	Calculated Integral
0	6.99	6.99
45	2.12	2.20
60	0.785	0.789
75	0.233	0.179

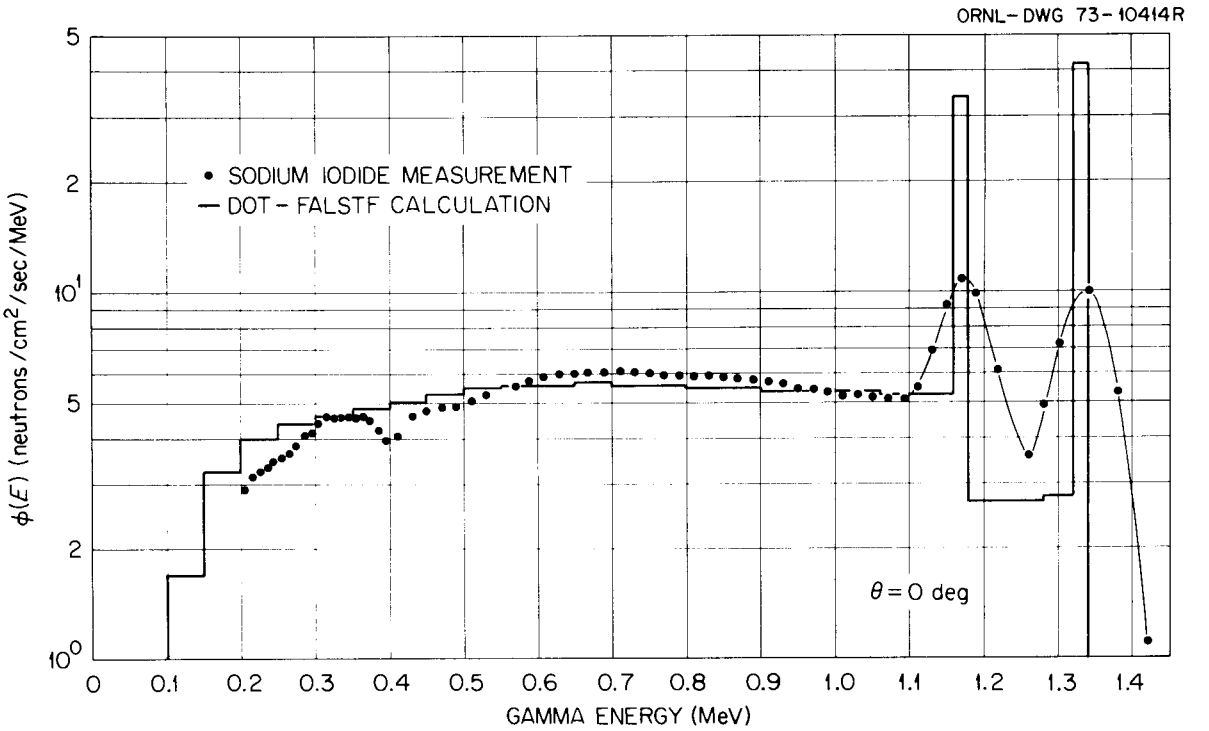

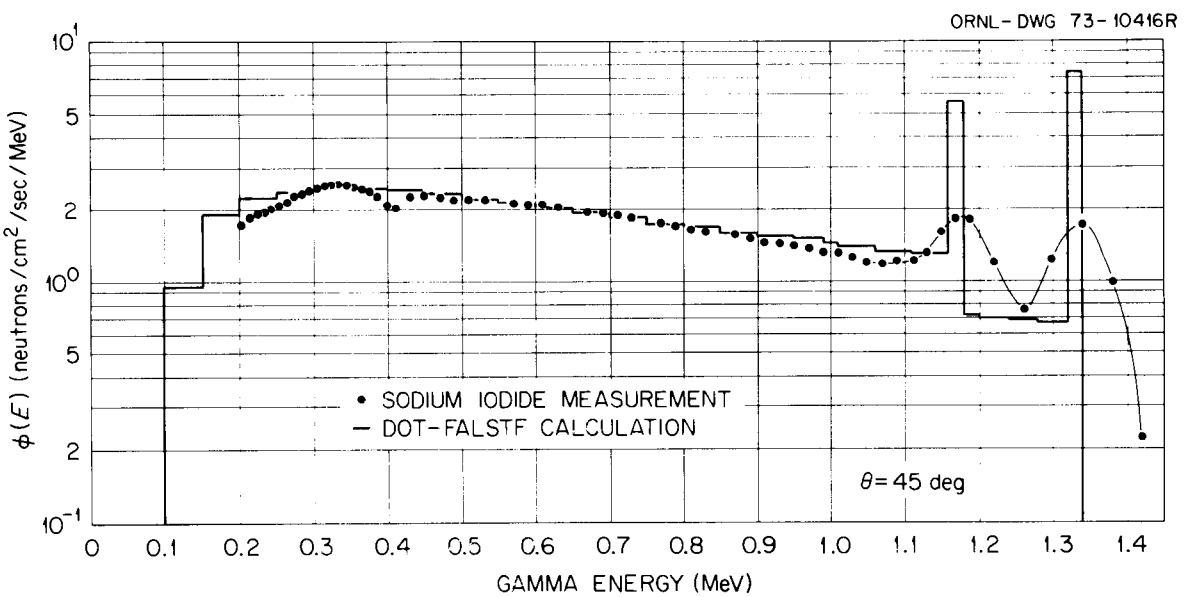

Fig. 6.5. Measured and Calculated Spectra of ^{60}Co Gamma Rays Emerging from Iron Slab at Angles of 0 and 45 deg (see Figs. 6.1 and 6.3).

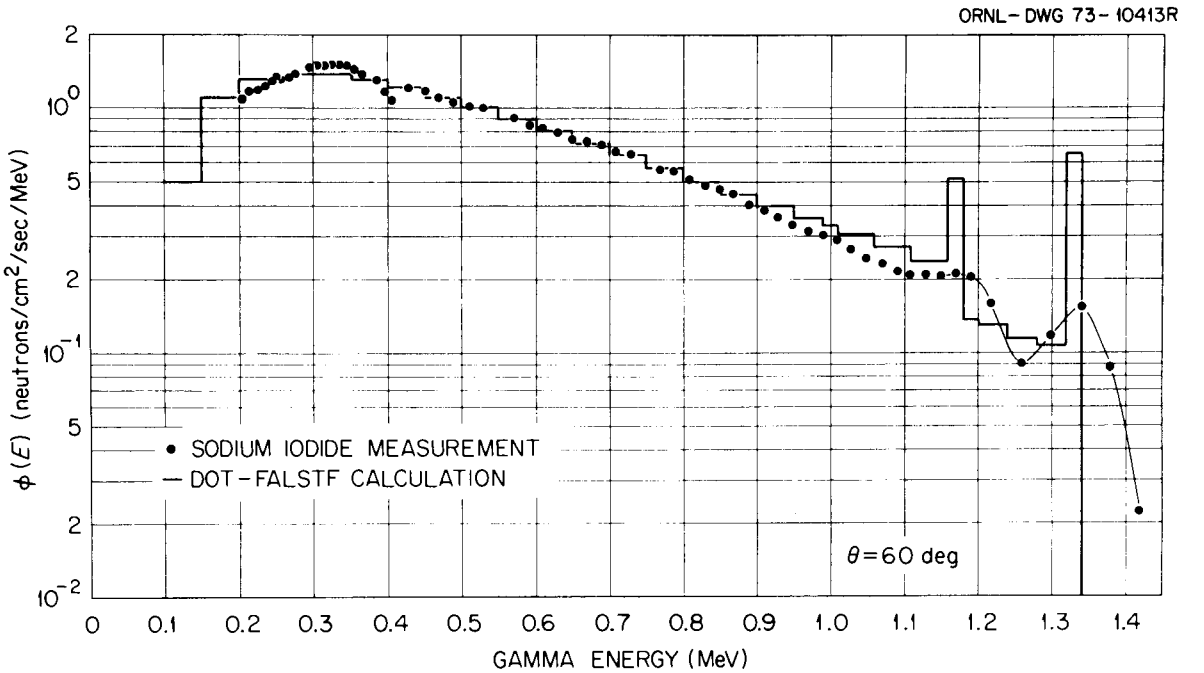

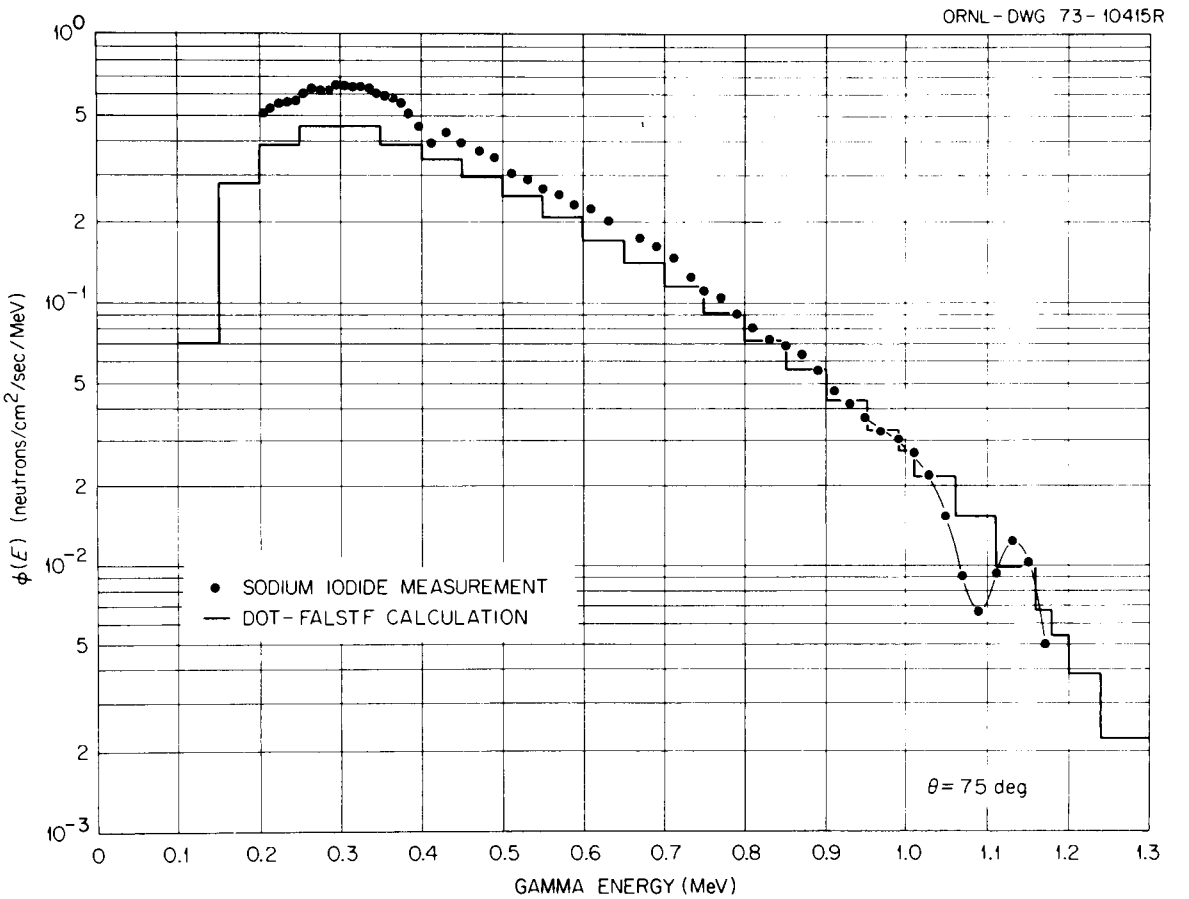

Fig. 6.6. Measured and Calculated Spectra of ^{60}Co Gamma Rays Emerging from Iron Slab at Angles of 60 and 75 deg (see Figs. 6.1 and 6.3).

Table 6.2. Calculated Spectra of Gamma Rays at Various Angles from ^{60}Co-Fe Configuration (see Fig. 6.3)

Energy Group	Energy (MeV)[a]			$\phi(E)\ \Delta E$ (γ's·cm^{-2}·sec^{-1})				$\phi(E)$ (γ's·cm^{-2}·sec^{-1}·MeV)			
	E_g	E_U	ΔE	0 deg	45 deg	60 deg	75 deg	0 deg	45 deg	60 deg	75 deg
1	1.33	1.34	2.0(-2)[b]	8.38(-1)	1.49(-1)	1.31(-2)	5.85(-6)	4.19(+1)	7.44(0)	6.67(-1)	2.93(-4)
2	1.30	1.32	4.0(-2)	1.09(-1)	2.68(-2)	4.28(-3)	3.21(-5)	2.79(0)	6.70(-1)	1.07(-1)	8.03(-4)
3	1.26	1.28	4.0(-2)	1.09(-1)	2.74(-2)	4.70(-3)	8.90(-5)	2.72(0)	6.85(-1)	1.17(-1)	2.23(-3)
4	1.22	1.24	4.0(-2)	1.09(-1)	2.80(-2)	5.15(-3)	1.56(-4)	2.72(0)	7.01(-1)	1.29(-1)	3.91(-3)
5	1.19	1.20	2.0(-2)	5.44(-2)	1.43(-2)	2.74(-3)	1.07(-4)	2.72(0)	7.13(-1)	1.37(-1)	5.36(-3)
6	1.17	1.18	2.0(-2)	6.76(-1)	1.13(-1)	1.03(-2)	1.36(-4)	3.38(+1)	5.64(0)	5.15(-1)	6.82(-3)
7	1.135	1.16	5.0(-2)	2.67(-1)	6.53(-2)	1.19(-2)	4.98(-4)	5.33(0)	1.31(0)	2.38(-1)	9.97(-3)
8	1.085	1.11	5.0(-2)	2.67(-1)	6.80(-2)	1.35(-2)	7.68(-4)	5.33(0)	1.36(0)	2.70(-1)	1.54(-2)
9	1.035	1.06	5.0(-2)	2.68(-1)	7.06(-2)	1.54(-2)	1.10(-3)	5.36(0)	1.41(0)	3.08(-1)	2.21(-2)
10	1.00	1.01	2.0(-2)	1.08(-1)	2.90(-2)	6.70(-3)	5.52(-4)	5.38(0)	1.45(0)	3.35(-1)	2.76(-2)
11	0.97	0.99	4.0(-2)	2.16(-1)	5.95(-2)	1.44(-2)	1.33(-3)	5.39(0)	1.47(0)	3.60(-1)	3.32(-2)
12	0.925	0.95	5.0(-2)	2.72(-1)	7.71(-2)	2.01(-2)	2.16(-3)	5.43(0)	1.54(0)	4.02(-1)	4.32(-2)
13	0.875	0.90	5.0(-2)	2.74(-1)	8.05(-2)	2.27(-2)	2.81(-3)	5.48(0)	1.61(0)	4.54(-1)	5.63(-2)
14	0.825	0.85	5.0(-2)	2.77(-1)	8.39(-2)	2.55(-2)	3.62(-3)	5.53(0)	1.68(0)	5.11(-1)	7.24(-2)
15	0.775	0.80	5.0(-2)	2.79(-1)	8.77(-2)	2.88(-2)	4.58(-3)	5.58(0)	1.76(0)	5.75(-1)	9.15(-2)
16	0.725	0.75	5.0(-2)	2.81(-1)	9.19(-2)	3.22(-2)	5.70(-3)	5.63(0)	1.84(0)	6.45(-1)	1.14(-1)
17	0.675	0.70	5.0(-2)	2.83(-1)	9.63(-2)	3.62(-2)	7.60(-3)	5.65(0)	1.93(0)	7.24(-1)	1.41(-1)
18	0.625	0.65	5.0(-2)	2.81(-1)	1.01(-1)	4.07(-2)	8.62(-3)	5.63(0)	2.03(0)	8.13(-1)	1.72(-1)
19	0.575	0.60	5.0(-2)	2.79(-1)	1.07(-1)	4.54(-2)	1.04(-2)	5.58(0)	2.13(0)	9.08(-1)	2.08(-1)
20	0.525	0.55	5.0(-2)	2.73(-1)	1.12(-1)	5.06(-2)	1.33(-2)	5.46(0)	2.24(0)	1.01(0)	2.50(-1)
21	0.475	0.50	5.0(-2)	2.64(-1)	1.17(-1)	5.60(-2)	1.48(-2)	5.28(0)	2.34(0)	1.12(0)	2.95(-1)
22	0.425	0.45	5.0(-2)	2.53(-1)	1.21(-1)	6.11(-2)	1.72(-2)	5.06(0)	2.41(0)	1.22(0)	3.45(-1)
23	0.375	0.40	5.0(-2)	2.43(-1)	1.23(-1)	6.58(-2)	1.96(-2)	4.86(0)	2.47(0)	1.32(0)	3.92(-1)
24	0.325	0.35	5.0(-2)	2.33(-1)	1.23(-1)	6.86(-2)	2.13(-2)	4.66(0)	2.46(0)	1.37(0)	4.27(-1)
25	0.275	0.30	5.0(-2)	2.22(-1)	1.19(-1)	6.86(-2)	2.15(-2)	4.44(0)	2.39(0)	1.37(0)	4.29(-1)
26	0.225	0.25	5.0(-2)	2.00(-1)	1.12(-1)	6.50(-2)	1.93(-2)	3.99(0)	2.24(0)	1.30(0)	3.87(-1)
27	0.175	0.20	5.0(-2)	1.62(-1)	9.47(-2)	5.48(-2)	1.41(-2)	3.25(0)	1.89(0)	1.10(0)	2.83(-1)
28	0.125	0.15	5.0(-2)	8.42(-2)	4.75(-2)	2.46(-2)	3.56(-3)	1.68(0)	9.50(-1)	4.91(-1)	7.12(-2)
29	0.075	0.10	5.0(-2)	1.95(-3)	5.62(-4)	9.25(-5)	2.31(-3)	3.89(-2)	1.12(-2)	∿ 0	∿ 0
30	0.030	0.05	4.0(-2)	∿ 0	∿ 0	∿ 0	∿ 0	∿ 0	∿ 0	∿ 0	∿ 0

[a] E_g = average energy in group; E_U = upper limit of energy; and ΔE = width of energy interval.

[b] Read: 2.0×10^{-2}.

With the probable explanation for the discrepancy at the 75-deg angle, these comparisons appear to validate the DOT calculational method for this experiment. Thus the discrepancies in the energy deposition results are probably due to some unknown factor either in the experimental technique or in our understanding of the TLD's themselves.

Section 6 References

1. F. R. Mynatt *et al.*, "Fast Reactor Analytical Shielding Progress Report for May and June 1973," ORNL-TM-4401, p. 70 (February 1974).

2. C. E. Clifford *et al.*, "Fast Reactor Experimental Shielding Monthly Progress Report for June 1973," ORNL-TM-4343, p. 4 (August 1973).

3. C. E. Clifford *et al.*, "Fast Reactor Experimental Shielding Monthly Progress Report for August and September 1973," ORNL-TM-4420, p. 5 (December 1973).

7. CALCULATIONS SUPPORTING THE DESIGN OF THE TSR-II LARGE-BEAM SHIELD

Work done by: S. Uchida, J. Lewin, and R. E. Maerker

With the low efficiencies of most radiation detectors, the reliability of flux and dose-rate measurements made behind thick shields depends on the strength of the source incident on the shield and on the intensity of the background in which the measurements are made. The demand for increasingly accurate experiments in the fast reactor shielding program conducted at the Tower Shielding Facility has prompted a recent study of a new design for a TSR-II beam shield which will both increase the number of neutrons incident on a test shield configuration and decrease the background due to neutrons that escape into the atmosphere. As part of this study, a series of calculations has been performed with the discrete ordinates code ANISN to predict the heating deposition and leakage dose rates that can be expected for each of several shield designs.[1]

The beam shield that has been used for the ORNL fast reactor shielding experiments performed to date consists of a 4-ft thickness of lead and water surrounding the spherically shaped TSR-II core. Originally constructed for experiments in which the reactor was operated above ground, the shield contains a beam port that is 10 in. in diameter over the first 24 in. from the core and 15 in. in diameter over the last 24 in. It has been adapted for fast reactor shielding experiments performed at ground level, but the number of neutrons available for an experiment is limited both by the beam port's relatively small cross section and by its relatively long length. Thus criteria for the new design include increasing the beam diameter and moving the shield test configuration closer to the core. At the same time, the design calls for less leakage through other regions of the shield than occurs with the present beam shield. Finally, the larger beam port requires an improved beam-shutter design to ensure protection from after-shutdown gamma rays.

To move the shield test configurations closer to the reactor and yet reduce the leakage into the atmosphere will require an asymmetrical shield.

Since reactor operation above ground is not necessary for these experiments, the shield can be a stationary structure into which the reactor vessel is lowered. Concrete was chosen for the bulk of the shield with layers of steel and water adjacent to the reactor vessel. The shield shape selected was a half-hexagon with the reactor located in the shield slightly off center of the full hexagon. A $\sim$ 3-ft-diam beam will emerge from the thin side of the shield.

In the first ANISN calculations the thick side of the shield was mocked up in spherical geometry for two proposed configurations (Cases 1 and 2 in Fig. 7.1). In each calculation the configuration was assumed to be adjacent to the outer surface of the reactor vessel, and the heat deposition throughout the shield was calculated for 1-MW operation. The calculations were performed with 21 neutron groups and 18 gamma-ray groups with P_3 scattering. The response functions were 39-group kerma factors taken from USAEC Report DLC-11. Figures 7.2 and 7.3 show the results.

As would be expected, Figs. 7.2 and 7.3 show that the energy deposition due to gamma rays is much greater than that due to neutrons. Also, the energy deposition for Case 2 is higher than that for Case 1, especially for distances out to 125 cm from the core center. A similar calculation for a configuration resembling that of the present shield (Case 3) yielded heat deposition results much like those for Case 1 (compare Figs. 7.2 and 7.4). When applied to calculations of the temperature distribution in the shields, no serious temperature gradients or heating problems were found to exist for any of the configurations.

Next, leakage dose rates for neutrons and gamma rays, including after-shutdown gamma rays, were calculated for all three configurations. As shown in Table 7.1, all the dose rates for Cases 1 and 2 are lower than those for Case 3; thus the background has indeed been reduced. To verify that background radiation will be significantly lower than the dose rates measured behind a test shield placed in the large beam, an additional calculation was performed for a postulated fast reactor shield configuration (Case 4). The dose rates shown in Table 7.1 for this case are indeed

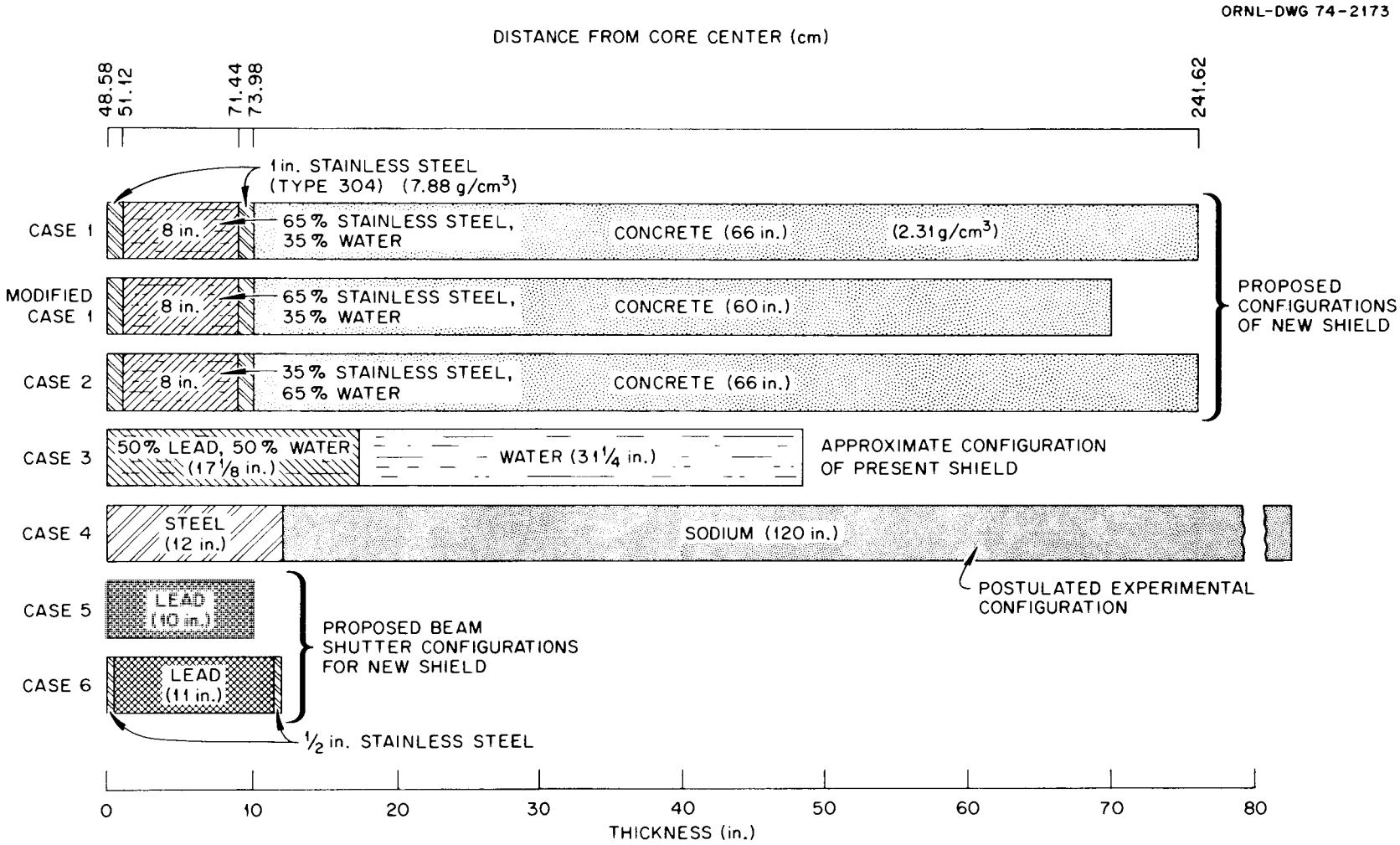

Fig. 7.1. Configurations Calculated in Support of TSR-II Large Beam Shield. Configuration begins at edge of reactor tank (at 48.58 cm from core center).

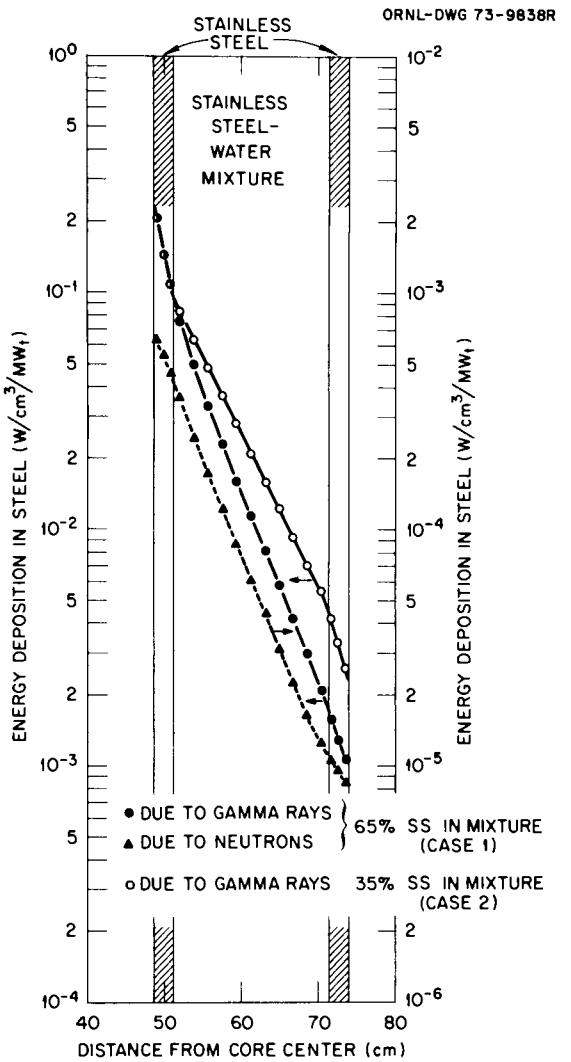

Fig. 7.2. Energy Deposition in Steel During 1-MW Operation (Cases 1 and 2)

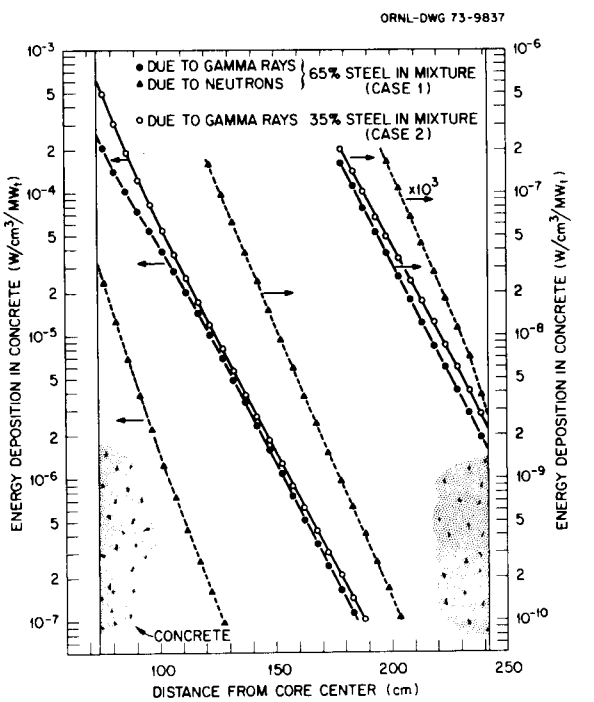

Fig. 7.3. Energy Deposition in Concrete During 1-MW Operation (Cases 1 and 2).

much higher than those for Cases 1 and 2 and thus background should not create a problem.

On the basis of these calculations and economic considerations, it was proposed that the thick side of the new beam shield have the configuration given for Case 1 but that the concrete thickness be reduced by 6 in. A calculation for the Modified Case 1 yielded at-power leakage dose rates that are higher than those for either Case 1 or Case 2 but lower than

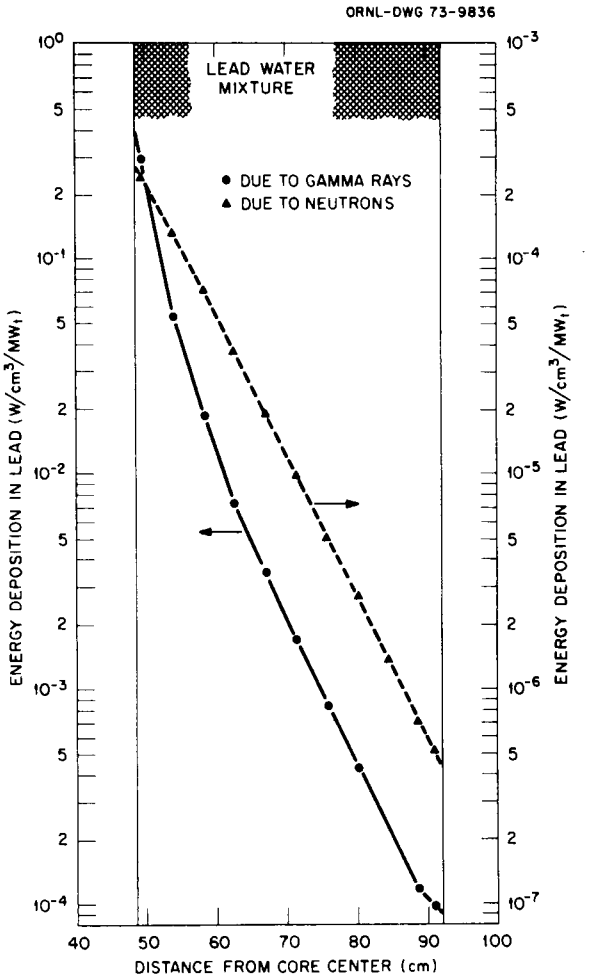

Fig. 7.4. Energy Deposition in Lead During 1-MW Operation (Case 3).

those for the present shield. The asymmetrical configuration as it is to be constructed is shown in Fig. 7.5. The relative size of the present shield is indicated by the dashed lines.

ANISN calculations were also performed for two configurations proposed for the beam-port shutter (Cases 5 and 6). The after-shutdown dose rate for Case 6 is the lowest and this configuration was proposed for the final shield. It will allow access in the vicinity of the beam port a few minutes after shutdown.

Table 7.1. Dose Rates at Outer Surface of Configurations During and After 1-MW Operation

Case No.	During Operation[a] Neutrons (mrem/hr/MW)	During Operation[a] Gamma Rays (mrem/hr/MW)	After-Shutdown Gamma Rays[b] (mrem/hr/MW)
1	5.5(1)[c]	3.09(2)	4.20(-1)
1 Mod.	5.0(2)	1.00(3)	1.58(0)
2	7.59(1)	4.72(2)	1.65(0)
3	8.83(2)	3.64(4)	2.11(1)
4	2.76(5)	1.06(5)	
5			5.79(2)
6			8.48(1)

[a]Subsequent to the reporting of these data results in Ref. 1, an error in a normalizing factor was discovered which would decrease the operating dose rates by about 17%.

[b]Immediately following four operational cycles consisting of 8 hr up, 16 hr down, and 8 hr up.

[c]Read as: 5.5×10^1.

ORNL-DWG 74-2174A

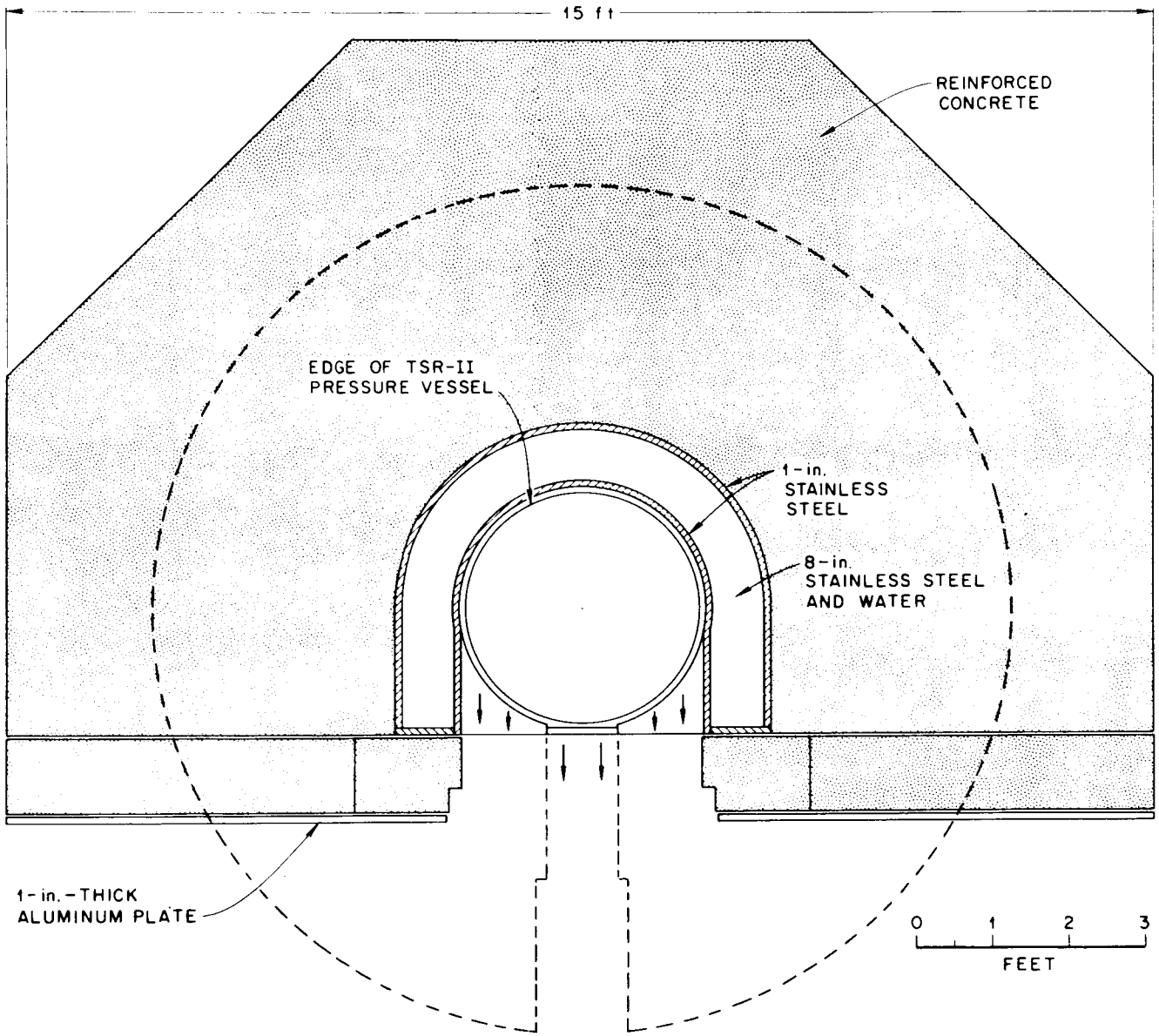

Fig. 7.5. Schematic of TSR-II Large-Beam Shield Through Horizontal Midplane.

Section 7 References

1. S. Uchida, J. Lewin, and R. E. Maerker, "Calculation of Energy Depositions and Dose Rates in Proposed Shielding Surrounding the TSR-II Reactor," ORNL-TM-4450 (January 1974).

ORNL-TM-4482
UC-79d - Liquid Metal Fast
Breeder Reactors Physics

INTERNAL DISTRIBUTION

1-3. L. S. Abbott
4. D. E. Bartine
5. G. T. Chapman
6. R. L. Childs
7-11. C. E. Clifford
12. M. B. Emmett
13. W. W. Engle, Jr.
14. G. F. Flanagan
15. R. M. Freestone, Jr.
16. W. O. Harms
17. G. Haynes
18. K. M. Henry
19. L. B. Holland
20. F. B. K. Kam
21. W. E. Kinney
22. J. Lewin
23. R. E. Maerker
24. F. C. Maienschein
25. F. J. Muckenthaler
26-30. F. R. Mynatt
31. E. M. Oblow
32. F. G. Perey
33. W. A. Rhoades
34. R. T. Santoro
35. H. E. Seagren
36. T. M. Sims
37. P. N. Stevens
38. J. H. Swanks
39. D. B. Trauger
40. D. K. Trubey
41. C. R. Weisbin
42. G. E. Whitesides
43. L. R. Williams
44. A. Zucker
45. H. Feshbach (consultant)
46. P. F. Fox (consultant)
47. W. W. Havens, Jr. (consultant)
48. A. F. Henry (consultant)
49-50. Central Research Library
51. ORNL Y-12 Technical Library
Document Reference Section
52-54. Laboratory Records Department
55. Laboratory Records ORNL RC
56. ORNL Patent Office

EXTERNAL DISTRIBUTION

57-58. USAEC Division of Reactor Research and Technology, Washington, D. C. 20545: Director.
59. USAEC-RRD Senior Site Representative, Oak Ridge National Laboratory, P. O. Box X, Oak Ridge, Tennessee 37830
60. USAEC Oak Ridge Operations Office, P. O. Box E, Oak Ridge, Tennessee: Research and Technical Support Division.
61-288. For distribution as shown in TID-4500 Distribution Category, UC-79d, Liquid Metal Fast Breeder Reactors Physics.